SUBMERGED FLOATING TUNNELS FOR AQUATOURISM

A Thesis

by

AMRITANSH PARTH

Submitted to the Office of Graduate and Professional Studies of
Texas A&M University
in partial fulfillment of the requirements for the degree of

MASTER OF SCIENCE

Chair of Committee,	John M. Niedzwecki
Committee Members,	Luciana Barroso
	H. Joseph Newton
Head of Department,	Robin Autenrieth

December 2015

Major Subject: Civil Engineering

ABSTRACT

In the last few years a rapid increase in the use of underwater space around the world has led to the development of a new field of tourism called “Aquatourism” or “Submerged Tourism”. This new field of aquatourism aims at providing a unique and unforgettable underwater viewing experience to general public any time of the year and for unlimited duration of time. As a part of aquatourism a new category of non-traditional transparent pedestrian tunnels is being proposed which are fully submerged in water. These pedestrian tunnels are envisioned to promote underwater tourism and recreational activities while at the same time act as permanent links across islands or undersea connections between specific underwater offshore sites and mainland.

This study aimed at understanding different floating and fixed bottom concepts for submerged tunnels. Using pure bending and coupled bending-torsion models the dynamic behavior of tunnel is studied. The use of acrylic plastic in combination with a steel spine has been investigated as a primary structural material for tunnel and key insights into the behavior of acrylic for circular and elliptical cross-sections have been developed and documented in the form of design charts. For evaluating hydrodynamic loads on the tunnel taking into account diffraction effects, Ogilvie’s Classical Solution has been used and the results compared with more general Morison’s equation. Finally, the response behavior of tunnel is simulated using purely analytical Modal Superposition Method and analytical/numerical Dynamic Stiffness Method.

Using structural and hydrodynamic models developed several parametric investigations have been done. The results of the parametric studies show how different structural and environmental parameters control the dynamic behavior of tunnel. The illustrative examples used for the numerical case studies show the suitability of different tunnel concepts based on site specific conditions and serviceability requirements. The numerical examples also show close agreement between the displacement values obtained using the modal superposition and the dynamic stiffness approach for response analysis.

By making use of first principles for model development and structural analysis, this study provides key insights into the behavior of submerged tunnels and would be useful in deciding important structural properties at the preliminary design assessment phase of these structures.

DEDICATION

To my parents

ACKNOWLEDGEMENTS

I would like to thank my committee chair, Dr. John M. Niedzwecki for his constant support, guidance and motivation throughout the course of this research. I would also like to thank my committee members, Dr. Luciana Barroso and Dr. H. Joseph Newton, for their valuable inputs in the due course of this research.

Thanks also go to my friends and colleagues and the department faculty and staff for making my time at Texas A&M University a great experience. Finally, thanks to my mother, father and sister for their encouragement and support.

TABLE OF CONTENTS

Page

LIST OF FIGURES

Page

LIST OF TABLES

Page

1. INTRODUCTION

The quest to understand the depths of sea and its unique occupants has always captured the imagination of mankind. This fascination with unknown has attracted millions of people to ocean looking for unique experiences. Over the period of years ocean depths have been explored by people from different fields; militaries around the world have used the sea for underwater missions; engineers and scientists have explored the ocean depths for minerals, energy, understanding of marine biology, geology and more; recreational divers have explored for sports, leisure activities and for getting a panoramic view of the marine world underneath. While recreational diving activity has attracted number of people all over the world, but owing to the constraints on duration of stay underwater, diving equipment and training needs, the opportunity to witness the panoramic submerged world is still not available to everyone. Subsequently, a rapid increase in the use of underwater space for recreational activities, around the world, has led to the development of new field of tourism called "Aquatourism" or "Submerged Tourism". This new field of "Aquatourism" aims at providing a unique and unforgettable underwater experience to general public without any space and time constraints [1]

In the last few years a continued interest in the field of "Submerged Tourism" has led to the development of new techniques and structures to experience the underwater habitats. These submerged structures provide an excellent tourism opportunity offering a variety of unique experiences like underwater dining and underwater observatory for getting an unobstructed view of marine flora and fauna. Some of the prominent structures constructed in this area are the Red Sea Star Restaurant in Eilat, Israel, ITHAA Hilton

Maldives Restaurant, San Sebastian Aquarium, Spain, Guangzhou Ocean World, China, Aquarium of the Americas, New Orleans, Greater Cleveland Aquarium, Cleveland, Ohio, Georgia Aquarium, Atlanta and Dubai Mall Aquarium.

The use of submerged structures for underwater restaurants is a relatively new concept and hasn't been implemented on a big scale. But the use of underwater tunnel aquariums has received great public attention considering the number of underwater aquaria's that have come up in the last few years. Most of these aquaria's are located onshore and are based on the traditional concept of a massive tank holding large amount of water and different forms of marine flora and fauna. The access to different areas of these aquariums is provided through underwater acrylic tunnels, giving a 360 degree view of the surrounding while walking through them (Figure 1). The hydrostatic pressure acting on the tunnel governs the structural design along with other considerations like tunnel span length and tunnel layout.

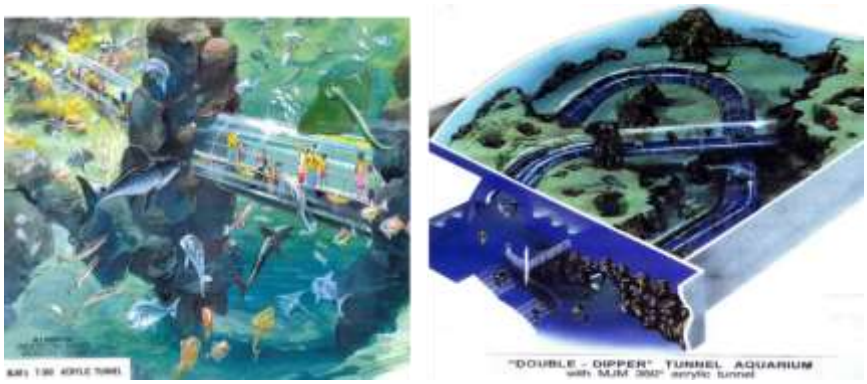

Figure 1 Traditional aquarium tunnels [2]

Although these underwater acrylic tunnels provide a unique near undersea experience, but the feeling of being right there in the middle of the ocean/water body is

still missing. Also, the cost of construction and the onshore space required for such aquariums is very large. Keeping this in view a new category of non-traditional aquarium tunnels is being proposed which are fully offshore. These offshore tunnels are motivated from the concept of a Submerged Floating Tunnel, which has been given a lot of attention in the recent years for establishing permanent connectivity across extreme crossings. In a way these Offshore Tunnels can be considered as smaller Floating Tunnel Systems spanning across a lake or connecting two islands (Figure 2). By using acrylic as structural material for these tunnels, they can not only serve as permanent pedestrian crossings but can also act as excellent tourist attractions providing a scenic view of the underwater world to people walking through them. These floating pedestrian tunnels will exhibit dynamic behavior and unlike traditional aquarium tunnels, where only hydrostatic pressure governs the structural design, the effect of waves and currents will also need to be accounted for in the design of these tunnels.

Figure 2 Non-traditional floating tunnel [3]

This study aims at understanding different smaller floating tunnels concepts for aquatourism and pedestrian application purpose. Use of acrylic as the primary structural

material for tunnel and the subsequent behavior of these non-traditional floating acrylic tunnels will be studied through simple analytical/numerical models. The study also focusses on the use of acrylic-steel combination as primary structural material and the resulting coupled bending-torsion behavior of tunnel. For external loading, the effect of hydrostatic pressure in selecting a suitable cross-sectional shape for acrylic tunnel will be evaluated. Finally, accounting for diffraction effects, environmental loads on the tunnel will be studied using Ogilvie's analytical solution for force on submerged circular cylinders and the results compared with force given by Morison's equation. The dynamic response of structure under the effect of regular waves will be studied using different analytical/semi-analytical approaches and parametric investigations done to understand the effect of key parameters on response behavior.

2. SUBMERGED FLOATING TUNNEL CONCEPTS

A submerged floating tunnel is conceived as a tube type of structure placed at a pre-determined depth below the surface of water. The unique feature of a submerged floating tunnel is that the buoyancy of water balances the dead load and live load of structure. The structure is held in position with the help of suitable anchoring arrangement, which essentially depends on the width of crossing and the water depth encountered. The anchoring system not only holds the structure in place but also provides the necessary stiffness against wave and current action. The concept of a Submerged Floating Tunnel or Archimedes Bridge dates back to 1886 when it was first brought by Sir James Reed of UK. The concept was further propagated in 1924 by Trygve Olsen Dale of Norway [4]. Since then much interest has been shown in the development of different SFT concepts by researchers from Norway, Italy, China and Japan. Many feasibility studies have been proposed discussing the possibility of SFT for Strait Crossing and crossing of deep and wide Fjords ([4], [5], [6], [7]). In Norway Høgsfjord Project was started in 1980's as the first major project for evaluating different SFT concepts. Four pre-qualified Norwegian contractors came up with four different SFT concepts. These concepts have been illustrated in Figure 3 and Figure 4 and important structural considerations summarized in Table 1.

Figure 3 SFT concepts for Høgsfjord Crossing [6]

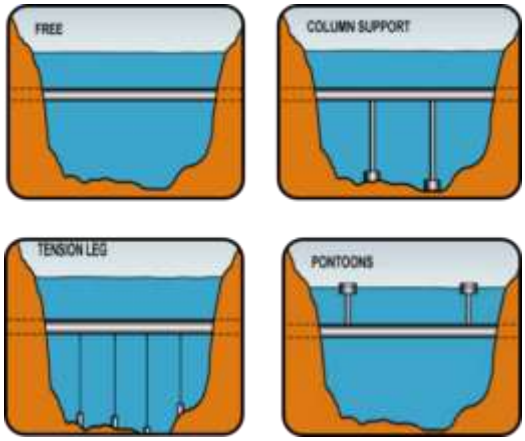

Figure 4 Floating tunnel concepts [6]

Table 1 SFT concepts and considerations

Sl No.	Anchoring System	Important Considerations
1	Free Floating Tunnel	• Tunnel has to be neutrally buoyant (BWR=1) • No limitation on water depth in which the tunnel can be used • Stability of tunnel becomes a key design issue for very wide crossings
2	Column Supported Tunnel	• Tunnel can be negatively buoyant (BWR<1) or neutrally buoyant (BWR=1) • The depth of water limits the use of this concept

Table 1 Continued

Sl No.	Anchoring System	Important Considerations
3	Tether Supported Tunnel	• Tunnel has to be positively buoyant (BWR>1) to maintain the tethers in tension • Tethers can be straight or inclined providing horizontal as well as vertical stiffness • Effective in both shallow water as well as deep water
4	Pontoon Supported Tunnel	• Tunnel has to be negatively buoyant (BWR<1). • Wind and wave considerations become important for this concept • No limitation on water depth in which the tunnel can be used

More recently a Sino-Italian joint venture (SIJLAB: Sino-Italian Joint Laboratory of Archimedes Bridge) has carried out the executive design of first SFT prototype to be installed in Qiandao Lake, China [8].

Over the last few years numerous studies have been done to study the dynamic behavior of Submerged Floating Tunnels under environmental loads. Most of these studies are numerical in nature and use finite element method for creating fluid-structure interaction model. Brancaleoni *et al.* [9] used a numerical approach to evaluate the dynamic behavior of a SFT using a coupled fluid-structure interaction model formulated using Morison's Equation. Remseth *et al.* [10] carried out the stochastic dynamic response analysis of SFT in time domain and frequency domain. They found that the effect of wave directionality, wave spreading and structural as well as hydrodynamic damping is

significant on dynamic response. Fogazzi and Perotti [11] carried out the dynamic analysis of seabed anchored SFT under seismic excitation. They developed an 'ad hoc' finite element for the anchor elements which accounted for geometrical non-linearities. Pilato *et al.* [12] further extended the application of 'ad hoc' finite element to a full 3D dynamic analysis of SFT. They took into account directional effects for surface waves and considered fully nonlinear form of Morison's equation for hydrodynamic loads. Accounting for slenderness and cross-sectional size of tunnel, effect of diffraction/radiation on the dynamic response of tunnel has also been studied by few researchers. Paik et al. [13] performed the dynamic analysis of SFT considering full radiation/diffraction problem. They used the Boundary Element Method to compute the wave potentials and further solved the dynamic equations in time domain. Ge et al. [14] also considered the radiation/diffraction effects for SFT but they solved the governing dynamic equations in frequency domain.

Apart from these numerical studies few experimental studies have been carried out to verify numerical results. In order to determine the best mooring configuration for a SFT under wave loading Kunisu *et al.* [15] carried out an experimental study and compared the results with numerical studies performed using Boundary Element Method and Morison's Equation. The results were in good agreement and showed that inclined tethers give better structural performance and the tether tension is directly related to the wave height. Long *et al.* [16] carried out a parametric study to evaluate the effect of different structural parameters on SFT response under hydrodynamic loads. Their results showed

that buoyancy-to-weight (BWR) ratio of the tunnel is a key parameter which governs the structural response.

The research studies reviewed until now use numerical approach to investigate the dynamic behavior. Few analytical studies have also been done for the assessment of response behavior. Sato *et al.* [17, 18] idealized a moored SFT as an Euler-Bernoulli beam on continuous elastic foundation. They further extended their work taking into account elasticity couplings. Additionally, they investigated a range of applicability within which beams on discrete elastic supports can be treated as beams on continuous elastic foundations. Tariverdilo *et al.* [19] idealized the SFT as an Euler-Bernoulli Beam on elastic foundation and used potential theory to get analytical expressions for the hydrodynamic loads. Dong *et al.*[20] took into consideration the curvature of the SFT and proposed dynamic equations for a spatially curved floating tunnel using Hamilton's principle.

Apart from these analytical studies done specifically for a Submerged Floating Tunnel, there is an abundance of literature on analytical models for similar structures like Floating Bridges. Fleischer and Park [21] idealized a beam floating on water surface as a Rayleigh beam and solved the hydroelastic free vibration and forced vibration problem using Fourier series expansion of mode shapes. They did not consider the radiation of surface waves while evaluating the hydrodynamic loads. Zhang *et al.* [22] investigated the dynamic behavior of floating bridges using beam theory for formulation of structural model and Boundary Element Method for evaluation of hydrodynamic loads. Analytical expressions for responses were obtained using Galerkin's Weighted Residual Method.

Newman [23] emphasized on the utility of mathematical mode shapes in the form of orthogonal polynomials for problems where natural modes shapes are affected by hydrodynamic pressure field.

The objective of most of the previous studies has been to study the global behavior of larger submerged floating tunnel systems under environmental and seismic actions. This study aimed at understanding smaller floating tunnels concepts for Aquatourism and pedestrian application purpose using simplified analytical approaches. Based on this a detailed discussion on the possible submerged tunnel concepts for pedestrian crossings, form and cross-sectional shape of these tunnels and the desired properties of the transparent structural material, has been carried out in detail in subsequent sections.

2.1. Submerged Tunnel Concepts for Pedestrian Crossings

The choice of submerged tunnel concept for pedestrian tunnels depends upon the geometrical characteristic of site like width of crossing and the water depth. The structures may span connecting two islands or span across a lake limiting the length of these tunnels between 20m-200m. Also, most of these structures will be located nearshore, hence shallow water assumption for water depth can be considered valid for these structures. Under these assumptions, the choice of submerged tunnel concepts deemed suitable for pedestrian tunnel application are Free Floating Tunnel, Column Supported Tunnel and Tethered Supported Tunnel.

The tunnel maybe in the form of a straight tube or some curvature may also be provided depending upon the site characteristic. In this study the case of a straight tunnel

has been considered. Possible mathematical formulation for each structural idealization has been discussed in detail in Section-3

2.2. Form and Cross-Sectional Shape

The form and cross-sectional shape of the tunnel determines its resistance ability to hydrostatic pressure. For some common underwater structures like the Pressure Hulls of Submarines, the preferred shape is a thin-walled circular cylinder. The reason for this as noted by Ross [24] is that the curved surface resists the pressure load in the form of uniform membrane stress acting all over the surface. For floating tunnels located offshore, apart from the hydrostatic pressure of water, additional loads on the structure will be due to wave and current action. From hydrodynamics point of view, the cross-sectional shape chosen should minimize the effect of wave and current loads on the structure. In addition, since the primary purpose of these tunnels is to promote underwater tourism, the choice of cross-sectional shape should enable the tunnel users to get an obstructed view of the underwater habitat.

Under these considerations, a circular cylindrical tunnel or an elliptical cylindrical cylinder can be considered as the most suitable cross-sectional shape for these floating pedestrian tunnels.

For traditional aquarium tunnels, circular cylindrical shapes are the most common ones with constant radius and 180 degrees span. For giving a more complete view of the underwater world the tunnels can span beyond 180 degrees sometimes. One disadvantage of using a circular cylinder form is that as the width of the cylinder gets wide, the clear space between visitors and top of tunnel increases. This leads to a lost feeling of being

underwater [25]. Use of elliptical cylindrical forms mitigates this issue giving them a more realistic underwater experience.

2.3. Materials

According to Ross [24] some of the important considerations to be taken into account while selecting a suitable material for underwater structures are ability to resist corrosion, strength/weight ratio, good sound absorption qualities, resistance to fire, material costs, ease of fabrication, operating life span of the material.

For submerged tunnel structures in particular, the structural material should withstand the external pressure loads and the continuous stress cycles due to action of waves and currents. Furthermore, since the tunnel stays in constant vicinity of water throughout its service life, the material should be able to withstand the corrosive action of water. Additionally, the material should also have good optical properties since the primary purpose of tunnels is to provide a complete view of the surrounding underwater habitat.

The use of Acrylic Plastic (Polymethyl Methacrylate, PMMA) as a structural material for aquarium glazing's and for window ports of submarine pressure hulls and pressure vessels has found a lot of acceptance over the period of years [26]. Owing to its structural as well as optical properties, Acrylic Plastic in combination with steel or concrete (Figure 5) can be considered as an excellent material for these floating pedestrian tunnels.

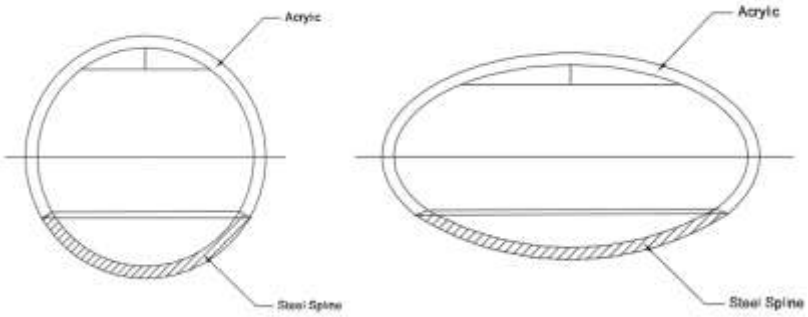

Figure 5 Use of acrylic-steel combination for tunnel cross-section

Designed properly, acrylic can not only provide excellent visibility but can also withstand static and dynamic loads of any magnitude. The key issue in the design of structural acrylic components is the choice of a safe design stress level that allows the component to function properly without the initiation of fracture. The value of this design stress level hasn't been codified until now. Hence, the designers have to rely on the published data and technical reports generated over the period of years to get the magnitude of safe design stress level [27]. Moreover, acrylic is a viscoelastic material i.e. the response of acrylic to stresses is nonlinear, dependent on both the temperature and the duration of stress application. Hence, the choice of a safe design stress level should take in to account the surrounding temperature and the duration of stress that the structural component needs to withstand. Stachiw [26] in his handbook on acrylics for aquaria's and semi submersibles summarizes the mechanical properties of acrylic. The summary has been presented in Table 3 and Table 4. In addition, the basic design parameters utilized for commercial design of acrylic components of underwater aquaria's are summarized in Table 2.

Table 2 Basic design parameters for acrylic used in aquaria's [28]

Elastic Modulus	3300 MPa
Poisson's Ratio	0.37
Safety Stress Permissible Water Side	3 MPa
Safety Stress Permissible Air Side	5 MPa
Density	1190 kg/m^3

Table 3 Minimum physical properties of acrylic meeting the requirements of the standard [27]

Test Procedures	Physical Property	Specified Values: U.S. Customary Unit	Specified Values: Metric Unit
ASTM D 256	Izod notched impact strength	≥0.25 ft-lb/in-min	≥13.3 J/m
ASTM D 570	Water absorption, 24 hr	≤0.25%	≤0.25%
ASTM D 621	Compressive deformation at 4,000 psi (27.6 MPa), at 122°F (50°C) 24 hr	≤1.0%	≤1.0%
ASTM D 638	Tensile:		
	(a) ultimate strength	≥9,000 psi	≥62 MPa
	(b) elongation at break	≥2%	≥2%
	(c) modulus	≥400,000 psi	≥2,760 MPa
ASTM D 695	Compressive:		
	(a) yield strength	≥15,000 psi	≥103 MPa
	(b) modulus of elasticity	≥400,000 psi	≥2,760 MPa
ASTM D 732	Shear ultimate strength	≥8,000 psi	≥55 MPa
ASTM D 785	Rockwell hardness	≥M scale 90	≥M scale 90
ASTMD 790	Flexural ultimate strength	≥14,000 psi	≥97 MPa
ASTM D 792	Specific gravity	0.043 lbs/in^3	1.19
ASTM E 308	Ultraviolet (290-330 nm) light Transmittance	≤5%	≤5%
ASTM D 696	Coefficient of linear thermal Expansion at 75°F (24°C)	42≤10^{-6} (in/in °F)	75.6≤10^{-6} (mm/mm °C)
ASTM D 648	Deflection temperature under Flexure at 264 psi (1.8 MPa)	≥185°F	≥85°C
PVHO-1 method, Para. 2-3.8	Total residual monomer: methyl methacrylate plus Ethyl acrylate	≤1.6%	≤1.6%

Table 4 Maximum allowable working stress levels for acrylic under long term loading (10 years) [27]

Temperature, ^{0}F (^{0}C)	Maximum Allowable Working Stress Level, psi	
	Tension (Column A)	Compression (Column B)
40 (4)	1900	6600
50 (10)	1800	6300
75 (25)	1500	5600
100 (38)	1200	5000
125 (52)	1100	4300
140 (60)	1000	3800
158 (70)	800	3200
175 (80)	600	2400
194 (90)	300	1800

Notes:
1 psi = 0.00689 MPa = 6.88 KPa = 6890 Pa
Acrylic castings per MIL-P-5425/ASME PVHO-1

3. MATHEMATICAL FORMULATIONS

3.1. Structural Bending Models for Free Spanning and Anchored Tunnels

The simplest configuration of a floating pedestrian tunnel is a freely spanning straight tunnel, connected only at the shores. The structure essentially behaves as a simply supported neutrally buoyant straight tunnel. For this configuration, under the assumption that the length of tunnel is much greater than the cross-sectional dimension, the tunnel can be idealized as a simply supported Euler-Bernoulli beam. The governing partial differential equation of motion describing the flexure behavior of the tunnel can then be expressed as [29]

$$EI\frac{\partial^4 v(x,t)}{\partial x^4}+m\frac{\partial^2 v(x,t)}{\partial t^2}=F(x,t) \tag{1}$$

where $v(x,t)$ is the displacement of the structure, m is the mass per unit length of beam including the added mass of water, I is the second moment of beam cross-section about the axis through the center of gravity of section, E is the modulus of elasticity of beam material, $F(x,t)$ is the external force acting on the beam cross-section which includes the hydrodynamic forces due to waves and current action.

For understanding the dynamic behavior of structure it is important to understand its natural modes of vibration. Floating Tunnel being a continuous system will have infinitely many natural modes of vibration. On excitation by a dynamic loading the structure will seek to vibrate in the natural mode having frequency close to the frequency of excitation. Hence, an estimate of natural frequency of the structure is required. This is

achieved through eigenvalue analysis of Eq.(1) using the method of separation of variable (Appendix-A).

The solution of Eq. (1) for free vibration case gives the analytical expression for natural frequencies of the system. The analytical expression as determined in Appendix-A is given as

$$\omega_n = \sqrt{\left(\frac{n\pi}{L}\right)^4 \frac{EI}{m}} \tag{2}$$

where n is the nth natural mode of vibration, m is the mass per unit length of beam including the added mass of water, I is the second moment of beam cross-section, E is the modulus of elasticity of beam material and L is the length of beam.

The natural modes of vibration of beam are given by

$$\Phi_n(x) = B_4 \sin\left(\frac{n\pi x}{L}\right) \tag{3}$$

where the constant B_4 can be evaluated using the property of orthogonality of natural modes and normalization of mode shapes.

The above formulation remains valid for tunnels which are neutrally buoyant. For the case of tunnels acted upon by net positive buoyant force (BWR>1), the net upward force on the structure can be balanced by providing tethers as shown in Figure 6

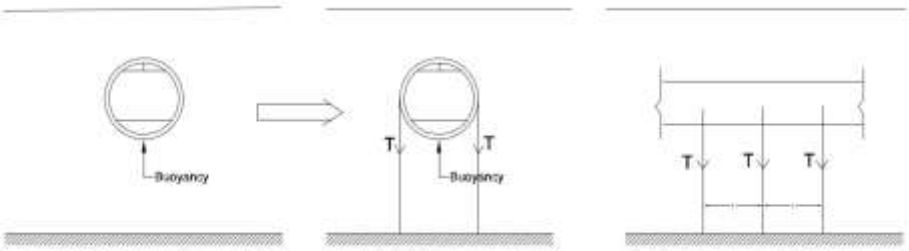

Figure 6 Tethered floating tunnel

The tension in tethers depends upon the net buoyant force acting on the tunnel. The tether arrangement can be vertical or inclined (Figure 7) depending on the stiffness required in horizontal and vertical direction.

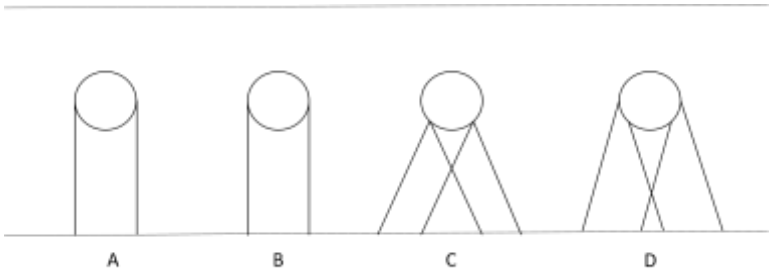

Figure 7 Different tether arrangements

The stiffness provided by tethers depends on several parameters: tether arrangement (Vertical/Inclined), angle of inclination in case of inclined tethers (θ from vertical), pre-tension in tethers (T_0), area of cross-section of tether (A), modulus of elasticity of tether material (E), length of tether (L_t). Based on these parameters, analytical expressions for tether stiffness have been developed for sway and heave motion of tunnel (Refer Appendix-B).

For Vertical Tether Arrangement,

Stiffness for Sway Motion of Tunnel

$$K_x = \frac{2T_o}{L_t} \tag{4}$$

Stiffness for Heave Motion of Tunnel

$$K_z = \frac{2AE}{L_t} \tag{5}$$

For Inclined Tether Arrangement,

Stiffness for Sway Motion of Tunnel

$$K_x = \frac{2AE}{L_t}\sin^2\theta \tag{6}$$

Stiffness for Heave Motion of Tunnel

$$K_z = \frac{2AE}{L_t}\cos^2\theta \tag{7}$$

The analytical expressions developed for tether stiffness can further be used to create a global structural model for tethered structure, idealizing the floating tunnel as a simply supported Euler-Bernoulli beam resting on discrete elastic supports. However, for this idealization closed-form analytical expressions for natural frequencies do not exist. Hence, a further simplification in the modeling assumption is done and the floating tunnel is further reduced as an Euler-Bernoulli beam resting on continuous elastic foundation (Figure 8).

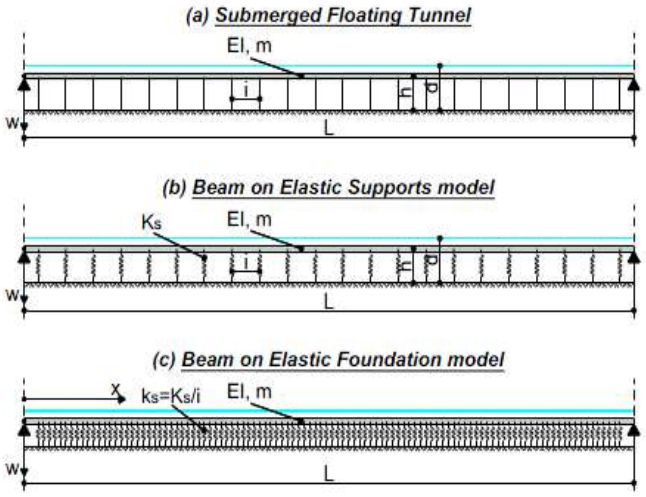

Figure 8 Structural idealization for tethered tunnel [30]

The applicability of stated assumption was studied by Sato *et al* [17, 18]. In the study they found that the natural modes and frequency of beam resting on continuous elastic foundation and the beam on discrete elastic support are similar for a range of parameter $K_v < 0.05$, where K_v is the relative stiffness parameter defined as,

$$K_v = \frac{K_s i^3}{24EI} \tag{8}$$

where k_s is the equivalent spring stiffness for tethers as determined in Appendix-B, i is the spacing between tethers and EI is the flexural rigidity of tunnel.

Now once the tunnel has been idealized as a beam resting on continuous elastic foundation, the governing partial differential equation of motion can be expressed as [29, 31]

$$EI\frac{\partial^4 v(x,t)}{\partial x^4} + m\frac{\partial^2 v(x,t)}{\partial t^2} + k_s v(x,t) = F(x,t) \tag{9}$$

The terms of Eq. (9) are similar to those in Eq. (1) with the only addition of k_s term, which is the equivalent tether stiffness defined as

$$k_s = \frac{K_s}{i}$$

where K_s is the actual tether stiffness defined by Eq. (4), Eq. (5), Eq. (6), Eq. (7), and i is the spacing between the tethers.

The free vibration analysis of the idealized system gives the closed-form expressions for natural frequencies and the corresponding mode shapes of vibration. The analytical expression for natural frequency as determined in Appendix-C is given by

$$\omega_n = \sqrt{\left(\frac{n\pi}{L}\right)^4 \frac{EI}{m} + \frac{k_s}{m}} \tag{10}$$

where n is the nth natural mode of vibration, m is the mass per unit length of beam including the added mass of water, I is the second moment of beam cross-section, E is the modulus of elasticity of beam material and L is the length of beam and k_s is the equivalent tether stiffness.

The corresponding mode shapes of vibration are given as

$$\Phi_n(x) = C_4 \sin\left(\frac{n\pi x}{L}\right) \tag{11}$$

where again the constant C_4 can be determined using the property of orthogonality of modes and normalization of mode shapes.

3.2. Dynamic Stiffness Model for Anchored Tunnels

The mathematical formulations for tethered tunnel discussed in (3.1) is valid only for certain range of values of relative stiffness parameter ($K_v < 0.05$). For cases when tethers cannot be idealized as continuous elastic foundation and have to be treated as discrete elastic supports, a separate analysis is required to determine the natural frequencies of structure.

Several methods exist in the literature to carry out eigenvalue analysis of Euler-Bernoulli beam resting on discrete elastic supports [32-36]

Rao [36] performed the free vibration analysis of a two span beam supported by intermediate elastic spring and clamped at the ends. In his analysis he treated the two spans separately and formulated the governing partial differential equation for each span. The solution of governing differential equations was carried out using end support boundary conditions and continuity condition at intermediate support for beam displacement, slope, bending moment and shear force. The method used by Rao resulted in 8x8 matrix of coefficients for a two span problem. The determinant of 8x8 matrix is further equated to zero to obtain the frequency equation, which is numerically solved to get the eigenvalues and the corresponding natural frequencies of system.

Although Rao's method works very well for a two-span system, but for bigger systems with many spans, the approach becomes computationally tedious due to rapid increase in the size of coefficient matrix. For solving these multiple span systems a computationally efficient approach is required. This leads us to Dynamic Stiffness Matrix Formulation [37]

Dynamic Stiffness Matrix is a single frequency dependent matrix which accounts for both mass and stiffness properties of the system. The element properties used in DSM is based on the exact closed form analytical solution of governing partial differential equation. Unlike the Finite Element Method, which interpolates displacement using natural polynomial shape functions, DSM uses frequency dependent shape functions to interpolate displacements. For system composed of multiple elements, the Dynamic Stiffness matrix of each element can be assembled together, likewise Finite Element Method, to form the global Dynamic Stiffness matrix of the system.

For Euler-Bernoulli beam shown in Figure 9 the element dynamic stiffness matrix relating the harmonically varying nodal forces to nodal displacements is given as [38, 39]

$$\begin{bmatrix} fy_1 \\ m_1 \\ fy_2 \\ m_2 \end{bmatrix} = \begin{bmatrix} d_1 & d_2 & d_4 & d_5 \\ d_2 & d_3 & -d_5 & d_6 \\ d_4 & -d_5 & d_1 & -d_2 \\ d_5 & d_6 & -d_2 & d_3 \end{bmatrix} \begin{bmatrix} \delta y_1 \\ \theta_1 \\ \delta y_2 \\ \theta_2 \end{bmatrix} \tag{12}$$

or simply

$$f = K(\omega)\delta \tag{13}$$

where f is the nodal force matrix, $K(\omega)$ is the frequency dependent dynamic stiffness matrix and δ is the nodal displacement matrix.

Figure 9 Euler-Bernoulli beam element with end forces and displacements

The terms of the dynamic stiffness matrix are given as

$$d_1 = \frac{W_3\lambda^3\left(\mathrm{S}_\lambda C_{h\lambda} + C_\lambda S_{h\lambda}\right)}{\Delta} \qquad d_2 = \frac{W_2\lambda^2 \mathrm{S}_\lambda S_{h\lambda}}{\Delta}$$

$$d_3 = \frac{W_1\lambda\left(\mathrm{S}_\lambda C_{h\lambda} - C_\lambda S_{h\lambda}\right)}{\Delta} \qquad d_4 = \frac{-W_3\lambda^3\left(\mathrm{S}_\lambda + S_{h\lambda}\right)}{\Delta}$$

$$d_5 = \frac{W_2\lambda^2\left(C_{h\lambda} - C_\lambda\right)}{\Delta} \qquad d_6 = \frac{W_1\lambda\left(\mathrm{S}_{h\lambda} - S_\lambda\right)}{\Delta}$$

with

$$\lambda = \left(\frac{m\omega^2 L^4}{EI}\right)^{1/4} \quad W_1 = \frac{EI}{L} \quad W_2 = \frac{EI}{L^2} \quad W_3 = \frac{EI}{L^3}$$

$$C_\lambda = \cos(\lambda) \quad S_\lambda = \sin(\lambda) \quad S_{h\lambda} = \sinh(\lambda) \quad C_{h\lambda} = \cosh(\lambda) \quad \Delta = 1 - C_\lambda C_{h\lambda}$$

Using the element dynamic stiffness matrix $K(\omega)$, the global stiffness matrix of a three span pedestrian tunnel shown in Figure 10 has been formulated and is given as

$$[K(\omega)]_{global} = \begin{bmatrix} d_3 & -d_5 & d_6 & 0 & 0 & 0 \\ -d_5 & 2d_1 + k_s & 0 & d_4 & d_5 & 0 \\ d_6 & 0 & 2d_3 & -d_5 & d_6 & 0 \\ 0 & d_4 & -d_5 & 2d_1 + k_s & 0 & d_5 \\ 0 & d_5 & d_6 & 0 & 2d_3 & d_6 \\ 0 & 0 & 0 & d_5 & d_6 & d_3 \end{bmatrix} \tag{14}$$

where k_s is the tether stiffness.

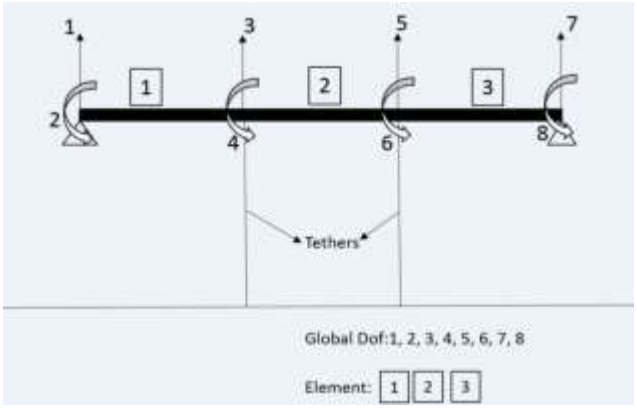

Figure 10 Global structural model for three span floating tunnel

It can be seen from Eq. (14) that even for a three span system the resulting dynamic stiffness matrix is a lower order 6x6 matrix. This stiffness matrix contains the mass and stiffness properties of the system and can be used to determine infinite number of eigenvalues of the system. Although, the case discussed here is for a three span floating tunnel system, the dynamic stiffness matrix can easily be expanded for more than three span systems without much computational effort.

The exact formulation of Dynamic Stiffness matrix for a beam element and the assembling of element stiffness matrix for a multispan beam has been discussed in detail in Appendix-D.

The natural frequencies of system is further computed by find the values of ω for which the determinant of global stiffness matrix vanishes. In this study this has been achieved by evaluating $\det[K(\omega)]$ at many values of ω and finding out the ω values at which the determinant value changes sign. More general algorithms like the Wittrick-William algorithm [40] can also be used for this purpose.

The dynamic stiffness formulation can also be used for pedestrian tunnel resting on rigid column supports. A column supported floating tunnel essentially behaves as an underwater bridge. The structure can be idealized as Euler-Bernoulli beam resting on discrete rigid supports as shown in Figure 11

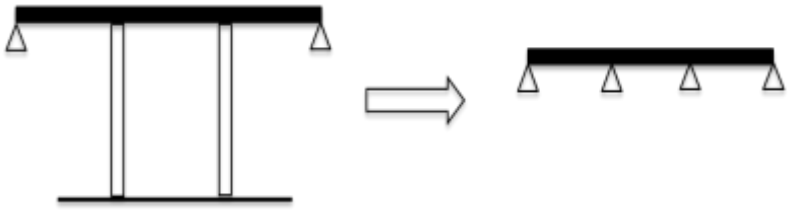

Figure 11 Structural idealization for a column supported floating tunnel

For a beam resting on discrete rigid supports, closed form-analytical solutions for natural frequency of system do not exist. Hence, a dynamic stiffness formulation is again used to carry out the free vibration analysis of the system.

The dynamic stiffness matrix formulated for a three span tethered SFT as formulated in previous section is given as,

$$[K(\omega)]_{global} = \begin{bmatrix} d_3 & -d_5 & d_6 & 0 & 0 & 0 \\ -d_5 & 2d_1 + k_s & 0 & d_4 & d_5 & 0 \\ d_6 & 0 & 2d_3 & -d_5 & d_6 & 0 \\ 0 & d_4 & -d_5 & 2d_1 + k_s & 0 & d_5 \\ 0 & d_5 & d_6 & 0 & 2d_3 & d_6 \\ 0 & 0 & 0 & d_5 & d_6 & d_3 \end{bmatrix}$$

For the case of tunnel resting on rigid column supports, the tether stiffness k_s in the global stiffness matrix can be approximated as approaching infinity ($k_s \to \infty$) to simulate a rigid support. For finding out the natural frequencies of system, again the values of ω

are determined at which the global stiffness matrix $K(\omega)$, with the tether stiffness term approaching infinity, vanishes. This is again achieved by evaluating $\det[K(\omega)]$ at many closely spaced values of ω within the frequency band of interest and noting the two ω values at which a sign change occurs.

3.3. Coupled Bending-Torsion Model for Acrylic-Steel Tunnels

Until now free vibration analysis of different floating tunnel configurations was carried for tunnel made of homogenous material with uniform mass distribution. The analysis was carried out under the assumption that tunnel is axisymmetric and the center of gravity of cross-section coincides with the shear center. This assumption led to a pure bending behavior of tunnel with no torsional rotations. However, the assumption of shear center and center of gravity coincidence fails for cross-section with only one axis of symmetry. This happens for floating tunnel sections made of combination of different materials e.g. Acrylic-Steel and Acrylic-Concrete combination as shown in Figure 12. The shift in the CG of cross-section away from the Shear Center leads to a coupled bending-torsion behavior of tunnel for sway and roll modes of vibrations. The axis passing through the shear center of cross-section is the elastic axis and through the mass center of cross-section is the inertial axis.

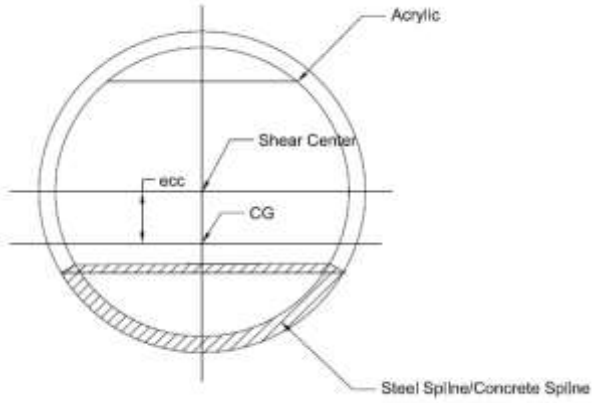

Figure 12 Cross-section with acrylic-steel combination (shear center offset)

. Depending on the eccentricity introduced and the length of tunnel, the extent of coupling on the dynamic behavior of structure is understood. The governing partial differential equations are formulated using the Euler-Bernoulli beam theory (for beam bending) and St. Venant's Theory of torsion (for beam torsion) and are expressed as [31]

$$\left(EI\right)_{eff}\frac{\partial^4 v}{\partial x^4}+\rho_{eff}A\frac{\partial^2\left(v+\mathrm{e}\phi\right)}{\partial t^2}=f\left(x,t\right) \tag{15}$$

$$-\left(GJ\right)_{eff}\frac{\partial^2\phi}{\partial x^2}+\rho_{eff}I_p\frac{\partial^2\phi}{\partial t^2}+\rho_{eff}Ae\frac{\partial^2\left(v+e\phi\right)}{\partial t^2}=f\left(x,t\right)e \tag{16}$$

where $v(x,t)$ is the displacement of structure in horizontal direction, ρ_{eff} is the equivalent density of material to ensure buoyancy-to-weight ratio as 1, I_p is polar moment of beam cross-section about elastic axis of section cross-section, A is the area of cross-section of beam, $(GJ)_{eff}$ and $(EI)_{eff}$ are the effective torsional and bending rigidities of cross-

section about the elastic axis of cross-section, ϕ is the torsion angle, e is the eccentricity introduced, $f(x,t)$ is the wave and current force acting in the horizontal direction.

For finding the mode shapes and natural frequency of vibration of structure, a free vibration analysis of structure is carried out using assumed modes method. The details of the free vibration analysis can be found in Appendix-E

The analytical expression for natural frequencies of system as determined in Appendix-E is given as

$$\omega_j^{\,2} = \frac{\left(p^2 + r^2\right) \mp \sqrt{\left(p^2 + r^2\right) + 4p^2 r^2 \left(q^2 e - 1\right)}}{2\left(1 - q^2 e\right)} \tag{17}$$

with

$$p^2 = \frac{(EI)_{eff}}{\rho_{eff} A}\left(\frac{n\pi}{L}\right)^4$$

$$q^2 = \frac{Ae}{I_p + Ae^2}$$

$$r^2 = \frac{(GJ)_{eff}\left(\frac{n\pi}{L}\right)^2}{\rho_{eff}\left(I_p + Ae^2\right)}$$

where n is the nth natural mode of vibration and L is the length of beam.

Eq.(17) gives two values of $\omega_j^{\,2}$, corresponding to two possible modes of coupled bending-torsion vibration.

3.4. Structural Loads

The loads acting on a submerged tunnel structure can be divided into Permanent Loads, Functional Loads, and Environmental Loads. The permanent loads are the loads due to dead weight of structure, the buoyant force acting on structure and the loads due to hydrostatic pressure of water. For traditional aquarium tunnels the external hydrostatic pressure governs the structural design of acrylic components that are used as viewports. While hydrostatic pressure is still an important component of permanent load for design of Floating Pedestrian Tunnels, it's the buoyancy-to-weight ratio (BWR) of the structure that acts as another important design parameter for Floating Tunnels.

The functional load acting on structure depends on the area of application of tunnel. For this study a floating tunnel for pedestrian application is being investigated, hence the load due to pedestrian movement is considered as the functional load on the structure.

For Floating Pedestrian Tunnels the environmental loads due to wave and current action is the most important parameter that governs the global behavior of structure. For accurate evaluation of wave and current loads on the structure, it is essential to determine site specific wave and current parameters.

For the three load categories, the procedure followed to evaluate loads and some important design considerations have been discussed in detail in the following sections.

3.5. Hydrostatic Pressure

Hydrostatic pressure of water at a given submergence depth is a permanent load acting on the structure and is an important parameter in the structural design of submerged

structures. Especially, for structures at greater water depths the effect of hydrostatic pressure cannot be ignored. For acrylic tunnels, in particular, hydrostatic pressure is an important consideration while deciding the thickness of acrylic panels that act as primary load bearing sections. For a structure immersed below the free surface of water the hydrostatic pressure is given by

$$P = \rho g H \tag{18}$$

where ρ is the density of water, g is the acceleration due to gravity and H is the depth below free surface.

As seen from Eq.(18) hydrostatic pressure at a section of submerged cylinder depends on the depth of section from the water surface and acts in the direction perpendicular to the section as shown in Figure 13.

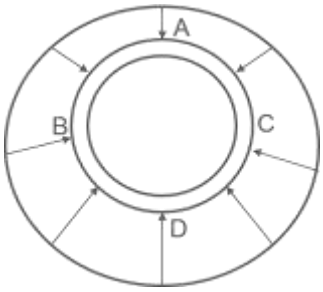

Figure 13 Distribution of hydrostatic pressure on circular cylinder

The hydrostatic pressure induces compressive stresses in the cross-section, which are resisted in the form of membrane stresses acting all over the surface. Under these compressive stresses the most critical modes of failure of circular cylindrical or elliptical cylindrical cross-sections are Axisymmetric Yield Failure, Shell Elastic Instability, Shell Inelastic Instability [24].

Depending upon the mechanical properties of structural material used for tunnel, length-diameter ratio and the thickness-radius ratio of tunnel, the critical buckling pressure for each failure mode can be determined using analytical expressions given by Bryan [41], Southwell [42], Winderburg and Trilling [43].

For a thin-walled circular cylinder under uniform lateral pressure the failure due to axisymmetric yielding occurs at a critical buckling pressure given by [24]

$$P_{cr} = \frac{\sigma_{yp} t}{a} \tag{19}$$

where σ_{yp} is the safe working stress of material, t is the wall thickness, a is the mean radius of circular cylindrical shell.

Under uniform external pressure, a thin-walled cylinder may buckle at a very small pressure as compared to pressure which causes axisymmetric yielding [24]. This failure mode of shell buckling is called the shell elastic instability. The critical buckling pressure for this mode of failure has been given by several authors. According to Bryan [41], the elastic instability pressure for an infinitely long cylinder is given by

$$P_{cr} = \frac{E}{4\left(1-\nu^2\right)}\left(\frac{t}{a}\right)^3 \tag{20}$$

where P_{cr} is the critical buckling pressure, t is the thickness of circular cylinder, a is the mean radius of circular cylindrical shell, E is the Young's Modulus, ν is the Poisson's ratio. Winderburg and Trilling [43] state that Eq.(20) applies to long, thin, perfect shaped tubes with no out-of-roundness

when

$$l > 4.9a\left(a/t\right)^{1/2} \quad \text{and} \quad a/t > 10$$

where l is the length of tube.

For shorter tubes supported at the ends, the buckling resistance is significantly increased. Winderburg and Trilling [43] summarized the analytical expression given by Von Mises for critical elastic instability pressure of short thin-walled circular cylinders under uniform lateral pressure given as

$$P_{cr} = \frac{1}{3}\left[n^2 - 1 + \frac{\lambda_1 n^4 - \lambda_2 n^2 + \lambda_3}{n^2 - 1} \right] \frac{2E}{1-\nu^2} \left(\frac{t}{D} \right)^3 + \frac{2E\left(\frac{t}{D} \right)}{(n^2 - 1)\left[n^2 \left(\frac{2L}{\pi D} \right)^2 + 1 \right]^2} \qquad (21)$$

with

$$\lambda_1 = \frac{\rho(2-\rho)}{(1-\rho)^2}$$

$$\lambda_2 = \rho\left[3 + \nu + \left(1-\nu^2\right)\rho \right]$$

$$\lambda_3 = \rho(1+\nu) - \rho^2 \left[\nu(1+2\nu) + \left(1-\nu^2\right)(1-\rho\nu)\left(1 + \frac{1+\nu}{1-\nu}\rho \right) \right]$$

$$\rho = \frac{1}{n^2 \left(\frac{2L}{\pi D} \right)^2 + 1}$$

where D is the diameter of cylinder, L is the length of cylinder, t is the wall thickness, P_{cr} is the critical buckling pressure, E is the modulus of elasticity, ν is the Poisson's ratio, n is the number of lobes or waves in a complete circumferential belt at the time of collapse (Figure 14)

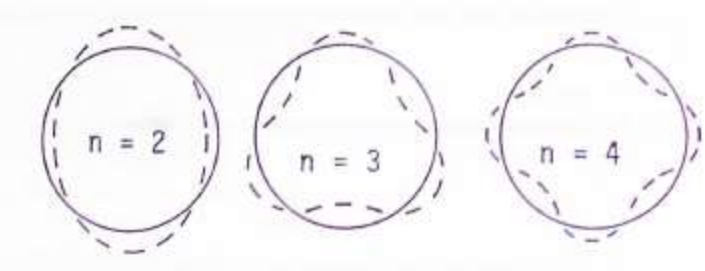

Figure 14 Circumferential wave patterns for buckling modes [24]

Neglecting higher powers of ρ Eq.(21) can be approximated as

$$P_{cr} = \frac{1}{3}\left[n^2 - 1 + \frac{2n^2 - 1 - \nu}{n^2\left(\frac{2L}{\pi D}\right)^2 - 1} \right] \frac{2E}{1-\nu^2}\left(\frac{t}{D}\right)^3 + \frac{2E\left(\frac{t}{D}\right)}{\left(n^2-1\right)\left[n^2\left(\frac{2L}{\pi D}\right)^2 + 1 \right]^2} \tag{22}$$

Southwell [42] using energy method came up with critical buckling pressure for shell instability as

$$P_{cr} = \frac{1}{3}\left(n^2-1\right)\frac{2E}{1-\nu^2}\left(\frac{t}{D}\right)^3 + \frac{2E\left(t/D\right)}{\left(n^2-1\right)n^4\left(\frac{2L}{\pi D}\right)^4} \tag{23}$$

For formulating each analytical expression for critical buckling pressure it was assumed that the cylinders have no initial out-of-roundness. However, Windenburg and Trilling [43] found that due to initial out-of-circularity/geometrical imperfections in cylinder, plasticity triggered off at some shell sections, lowering the critical buckling pressure than the value predicted by Eq.(21), Eq.(22), Eq.(23). To take into account the initial out-of-roundness Winderburg and Trilling [43] introduced their thinness ratio λ

which can be used to determine the plastic reduction factor (PKD) using the design chart given in Figure 15.

$$\lambda = \left[\left(\frac{L}{D} \right)^2 / \left(\frac{t}{D} \right)^3 \right]^{1/4} \sqrt{\sigma_{yp} / E} \tag{24}$$

Once the plastic reduction factor is determined, the predicted buckling pressure can be evaluated using

$$P_{pred} = \frac{P_{cr}}{PKD} \tag{25}$$

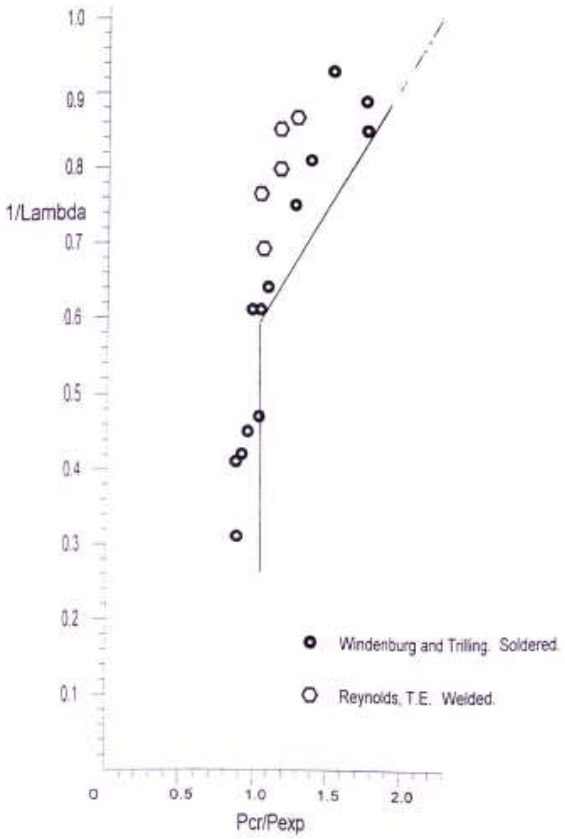

Figure 15 Design chart for PKD [24]

Using analytical expressions for critical buckling pressure, a design curve is prepared for critical buckling pressure as a function of thickness-radius ratio of circular cylinder for a given length-diameter ratio. The design curve can further be used to decide the thickness of acrylic panels for submerged circular cylindrical tunnel cross-sections, effective to resist the hydrostatic pressure at a given depth of submergence.

The critical buckling pressure discussed until now are for circular cylinders with no out-of-roundness or for cylinders with slight initial out-of-roundness. Winderburg and Trilling [43] showed that critical buckling pressure for tubes with slight initial imperfection is lower than that for a perfect circular cylinder. For case of tubes with initial ellipticity/ovality as shown in Figure 16 there is a further severe reduction in the critical buckling pressure.

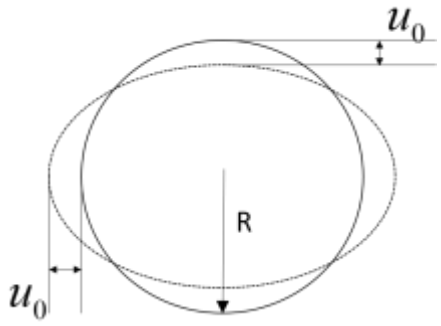

Figure 16 Tubes with an initial ellipticity

This reduction in critical pressure depends on the magnitude of initial ovality with respect to mean radius of perfect circular cylinder. Timoshenko [44] has shown that the maximum stress acting on the wall of an elliptical cross-section is given by

$$|\sigma|_{\max} = \frac{PR}{t} + \frac{6PRu_0}{t^2}\frac{1}{1-\frac{P}{P_{cr}}} \tag{26}$$

where R is the mean cylinder radius, t is the wall thickness, P_{cr} is the critical buckling pressure of perfect circular cylinder, u_0 is the initial ovality, P is the external pressure, $|\sigma|_{\max}$ is the maximum stress which for the limiting value of external pressure P is the safe design working stress of material. Once the safe design working stress of material is known, Eq.(26) can used to determine the limiting pressure at which material yielding starts. Substituting, $\frac{R}{t} = m$ and $\frac{u_0}{R} = n$ in (26) we get

$$P_L^{\,2} - \left[\frac{\sigma_s}{m} + (1+6mn)P_{cr}\right]P_L + \frac{\sigma_s P_{cr}}{m} = 0 \tag{27}$$

where P_L is the limiting pressure corresponding to safe design stress σ_s of material and P_{cr} is the critical buckling pressure for perfect circular cylinder.

Solution of Eq.(27) gives the critical limiting pressure for elliptical cylinders corresponding to the safe design stress of material.

3.6. Functional Loads

The pedestrian movement on the tunnel causes both static and dynamic loads on the structure. For evaluating pedestrian loads guidelines of LRFD Specification for the Design of Pedestrian Bridges has been followed in this study. The pedestrian tunnel shall be designed for a uniform pedestrian loading of 90 psf with a load factor of 1.75, patterned to produce maximum load effects. Vibrations due to pedestrian movement shall also be

investigated as a service limit state. The fundamental frequency in a vertical mode of tunnel without live load shall be greater than 3Hz to avoid the first harmonic. For the lateral mode the fundamental frequency shall be greater than 1.3Hz. If the fundamental frequencies do not meet these limits, evaluation of dynamic performance shall be made

3.7. Environmental Loads

For evaluating environmental loads on a Submerged Floating Tunnel several approaches have been used until now. Of all the approaches, Morison's equation is the simplest one and has been used by several authors [8-10, 15]. The application of Morison's equation is valid for cases when the ratio of characteristic cross-section dimension of the structure and the wavelength is small, typically less than 0.1. For higher values of this ratio, diffraction effects have to be taken into account. Using the diffraction theory under potential flow regime, the inertial forces acting on a SFT has been evaluated by Kunisu *et al.* [15] and F. Ge *et al.* [14]. Both the studies adopted a numerical approach using Boundary Element Method for evaluating the diffraction/radiation potentials and the corresponding inertial forces acting on the structure.

While the application of Boundary Element Method gives a good estimate of wave force, but its implementation takes a lot of time and computational effort. For this reason simplified analytical expressions based on Ogilvie's classical solution [45] has been used for evaluating the first-order forces on floating pedestrian tunnels in this study. The analytical expressions are valid under the assumption that the floating tunnel has a circular-cross section and is restrained from moving. First-order forces from Ogilvie's

solution are then compared with the force evaluated using Morison's equation under linear theory assumption for wave kinematics.

Idealizing the Submerged Floating Tunnel as a circular cylinder of radius a, submerged at a depth h below the free surface (Figure 17) in a water body of infinite depth.

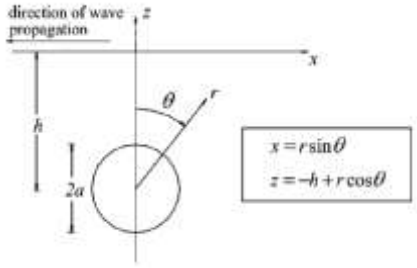

Figure 17 Tunnel cross-section under regular wave

For incoming regular waves of amplitude A , wave number K , and frequency ω , the incident velocity potential in Cartesian coordinates, can be written as the real part of

$$\phi_I = \frac{Ag}{\omega}\exp\left(Kz - iKx - i\omega t\right) \tag{28}$$

For the case of a circular cylinder Eq.(28) can be written in a cylindrical coordinate system (r,θ,z) as

$$\phi_I = \mathrm{Re}\left(\frac{Ag}{\omega}\exp\left(-Kh\right)\exp\left(Kr\exp\left(-i\theta\right)\right)\exp\left(-i\omega t\right)\right) \tag{29}$$

The free surface elevation is then given as

$$\eta_I\left(x,t\right) = -\frac{1}{g}\frac{\partial\phi_I}{\partial t} = A\sin\left(Kx + \omega t\right) \tag{30}$$

The total velocity potential of diffracted wave is obtained by summing up the contribution from incident potential and scattered velocity potential. The total first order

velocity potential of the diffracted wave field has been given by Arena [46] using multipole expansion as

$$\phi_D = \frac{Ag}{\omega}\exp(-Kh)\left[-P(r,\theta,\omega)\sin(\omega t)+Q(r,\theta,\omega)\cos(\omega \mathrm{t})\right] \tag{31}$$

where

$$P(r,\theta,\omega)=\frac{1}{1+S_\varepsilon{}^2}\left[\sum_{n=1}^{\infty}\varepsilon_n D_n\left(\sin(n\theta)-S_\varepsilon\cos(n\theta)\right)+\sum_{n=1}^{\infty}n\varepsilon_n\left(S_\varepsilon A_n-B_n\right)\right] \tag{32}$$

$$\mathrm{Q}(r,\theta,\omega)=1+\frac{1}{1+S_\varepsilon{}^2}\left[\sum_{n=1}^{\infty}\varepsilon_n D_n\left(\cos(n\theta)+S_\varepsilon\sin(n\theta)\right)-\sum_{n=1}^{\infty}n\varepsilon_n\left(A_n+S_\varepsilon B_n\right)\right] \tag{33}$$

In Eq.(32) and Eq.(33) $\varepsilon_n(\mathrm{Ka},\mathrm{Kh})$ are the solutions of equations given by

$$\varepsilon_n+(Ka)^{2n}\sum_{m=1}^{\infty}\frac{(n+m)!}{n!(m-1)!}A_{n+m}\varepsilon_m=\frac{(Ka)^{2n}}{n!} \tag{34}$$

The functions $A_n, B_n, D_n, S_\varepsilon$ in Eq.(32) and Eq.(33) are defined as

$$A_n(Kh)=\frac{1}{n(2Kh)^n}+\frac{2}{n!}\left[\exp(-2\mathrm{Kh})\,\mathrm{P}\int_{-\infty}^{2Kh}\frac{\exp u}{u}du-\sum_{m=1}^{n}\frac{(m-1)!}{(2Kh)^m}\right] \tag{35}$$

with $n\geq 1$ and P is the Cauchy's principal value of the integral.

$$B_n(Kh)=\frac{2\pi\exp(-2Kh)}{n!} \tag{36}$$

$$D_n(Kr,Ka)=\frac{1}{(\mathrm{Kr})^n}+\frac{(Kr)^n}{(Ka)^{2n}} \tag{37}$$

$$S_\varepsilon(Ka,Kh)=2\pi\exp(-2Kh)\sum_{n=1}^{\infty}\frac{\varepsilon_n}{(n-1)!} \tag{38}$$

Using the velocity potential of diffracted wave field defined in Eq.(31) the pressure variation acting over the boundary of cylinder is evaluated using

$$\Delta p = -\rho \frac{\partial \phi_D}{\partial t} \tag{39}$$

Subsequently, the force acting on the cylinder is obtained by integrating the pressure variation over the boundary of the cylinder.

The first-order component of force acting in x-direction is expressed as

$$F_x = \rho a \int_0^{2\pi} \Delta p \sin\theta d\theta = \frac{-2\pi\rho g A}{K} \exp(-Kh) \varepsilon_1 \left(1 + S_\varepsilon{}^2\right)^{-1/2} \cos(\omega t - \varphi) \tag{40}$$

Similarly, the first-order component of force acting in z-direction is expressed as

$$F_z = \rho a \int_0^{2\pi} \Delta p \cos\theta d\theta = \frac{-2\pi\rho g A}{K} \exp(-Kh) \varepsilon_1 \left(1 + S_\varepsilon{}^2\right)^{-1/2} \sin(\omega t - \varphi) \tag{41}$$

where

$\varphi = \tan^{-1}(S_\varepsilon)$

From Eq.(40) and Eq.(41) it is evident that the magnitude of force in horizontal direction (x-axis) is equal to the magnitude of force in vertical direction (z-axis). The only difference is that vertical force is 90° out-of-phase of the horizontal force.

Once the total loading on the structure is determined, the response of the structure can be evaluated using suitable analytical approaches discussed in subsequent sections.

3.8. Modal Superposition Method for Response Analysis

For a floating tunnel under external excitation due to wave loading the governing equation describing the motion of tunnel is given by

$$EI\frac{\partial^4 v(x,t)}{\partial x^4}+m\frac{\partial^2 v(x,t)}{\partial t^2}=F(x,t) \tag{42}$$

The external excitation force due to wave loading can be described by Morison's equation as,

$$F(x,t)=\frac{1}{2}\rho_w C_D D\left(v_w-\dot{v}\right)\left|v_w-\dot{v}\right|+\rho_w C_M\frac{\pi D^2}{4}a_w-\rho_w\left(C_M-1\right)\frac{\pi D^2}{4}\ddot{v} \tag{43}$$

where ρ_w is the water mass density, D is the outer diameter of the tunnel, C_D is the drag coefficient, C_M is the inertia coefficient, v_w is fluid particles velocity vector, a_w is fluid particles acceleration vector, $\dot{v}$ is structure velocity, $\ddot{v}$ is structure acceleration.

From Eq.(43) it can been seen that the drag part of Morison's equation is non-linear. Under the assumption that for a submerged floating tunnel, at a given depth below free surface, the structure velocity is small in comparison to the fluid particle velocity, the non-linear part of Eq.(43) can be linearized and equation can be rewritten as

$$F(x,t)=\frac{1}{2}\rho C_D D\left[v_w\left|v_w\right|-2\left\langle\left|v_w\right|\right\rangle\dot{v}\right]+\rho C_M\frac{\pi D^2}{4}a_w-\rho\left(C_M-1\right)\frac{\pi D^2}{4}\ddot{v} \tag{44}$$

where $\left\langle\left|v_w\right|\right\rangle$ is the time averaged fluid particle velocity.

Substituting Eq.(44) in Eq.(42) and rearranging the terms on left hand side we get

$$\begin{aligned}EI\frac{\partial^4 v(x,t)}{\partial x^4}+\left(m+\rho\frac{\pi D^2}{4}\left(C_M-1\right)\right)\frac{\partial^2 v(x,t)}{\partial t^2}+\left(\rho C_D D\left\langle\left|v_w\right|\right\rangle\right)\frac{\partial v}{\partial t}\\ =\frac{1}{2}\rho C_D D v_w\left|v_w\right|+\rho C_M\frac{\pi D^2}{4}a_w\end{aligned} \tag{45}$$

Assuming that the tunnel is simply supported at the ends, the total displacement $v(x,t)$ can be expanded into respective modal contributions as

$$v(x,t)=\sum_{n=1}^{\infty}\sin\left(\frac{n\pi x}{L}\right)q_n(t) \tag{46}$$

The excitation term on the right hand side of Eq.(45) can be written as

$$\frac{1}{2}\rho C_D D v_w|v_w|+\rho C_M\frac{\pi D^2}{4}a_w=F_1\sin(\omega t)+F_2\cos(\omega t) \tag{47}$$

where F_1, F_2 and ω depend on wave parameters (See Appendix-F)

Substituting Eq.(46) and Eq.(47) in Eq.(45) we get

$$EI\sum_{n=1}^{\infty}\left(\frac{n\pi}{L}\right)^4\sin\left(\frac{n\pi x}{L}\right)q_n(t)+M_t\sum_{n=1}^{\infty}\sin\left(\frac{n\pi x}{L}\right)\ddot{q}_n(t)+C\sum_{n=1}^{\infty}\sin\left(\frac{n\pi x}{L}\right)\dot{q}_n(t) = F_1\sin(\omega t)+F_2\cos(\omega t) \tag{48}$$

with

$$M_t=\left[m+\rho\frac{\pi D^2}{4}(C_M-1)\right]$$

$$C=\rho C_D D\langle|v_w|\rangle$$

Multiplying both sides of Eq.(48) by $\sum_{m=1}^{\infty}\sin\left(\frac{m\pi x}{L}\right)$, integrating the resulting expression from 0 to L and utilizing the property of orthogonality of modes we get

$$EI\left(\frac{L}{2}\right)\left(\frac{n\pi}{L}\right)^4 q_n(t)+M_t\left(\frac{L}{2}\right)\ddot{q}_n(t)+C\left(\frac{L}{2}\right)\dot{q}_n(t)=P_n(t) \tag{49}$$

with

$$P_n(t) = \frac{L}{n\pi}\left(F_1 \sin(\omega t) + F_2 \cos(\omega t)\right)\left(1 - \cos(n\pi)\right)$$

Eq.(49) is simplified and written as

$$\ddot{q}_n(t) + \frac{C}{M_t}\dot{q}_n(t) + \omega_n{}^2 q_n(t) = \frac{2P_n(t)}{M_t L} \tag{50}$$

From Eq.(50) we can see that the governing partial differential equation Eq.(45) for tunnel displacement $v(x,t)$ has been transformed in to infinite set of ordinary differential equation for each mode of beam vibration. The total displacement $v(x,t)$ is further obtained using Eq.(46)

The damping term in Eq.(50) is the sum of structural damping and the hydrodynamic damping and is non-proportional in nature. This implies that,

$$\frac{C}{M_t} \neq 2\zeta\omega_n \tag{51}$$

Numerical integration of Eq.(50) is required to solve the ordinary differential equation. However, under the assumption that damping is very small and neglecting the damping component of Eq.(50), the steady state analytical solution of the resulting equation can be expressed as

$$q_n(t) = \frac{4F_1}{\pi M_t}\left(\frac{1}{\omega_n{}^2 - \omega^2}\right)\sin(\omega t) \tag{52}$$

where ω_n is the n^{th} natural frequency and ω is the frequency of the forcing function.

Using Eq.(52) and Eq.(46) the total steady state displacement $v(x,t)$ can be expressed as

$$v(x,t)=\sum_{n=1}^{\infty}\frac{4F_1}{\pi M_t}\left(\frac{1}{\omega_n{}^2-\omega^2}\right)\sin(\omega t)\sin\left(\frac{n\pi x}{L}\right) \tag{53}$$

3.9. Dynamic Stiffness Method for Time Domain Response Analysis

For the three span continuous floating tunnel resting on tethered supports (Figure 18), the governing equation of motion was formulated in 3.2 using dynamic stiffness matrix.

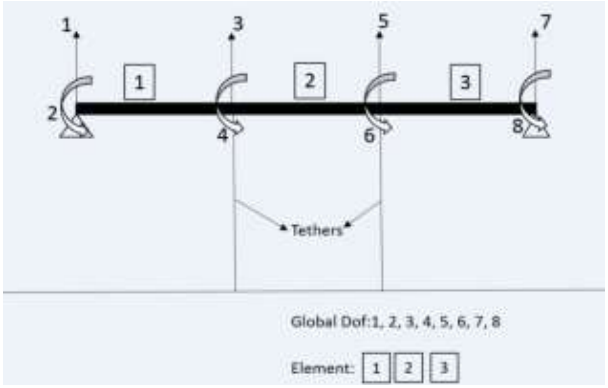

Figure 18 Global model for dynamic stiffness matrix

For a harmonically varying force acting at the nodes of beam, beam end displacements can be expressed as

$$\begin{bmatrix}\theta_2\\ \delta_3\\ \theta_4\\ \delta_5\\ \theta_6\\ \theta_8\end{bmatrix}=\begin{bmatrix} d_3 & -d_5 & d_6 & 0 & 0 & 0\\ -d_5 & 2d_1+k_s & 0 & d_4 & d_5 & 0\\ d_6 & 0 & 2d_3 & -d_5 & d_6 & 0\\ 0 & d_4 & -d_5 & 2d_1+k_s & 0 & d_5\\ 0 & d_5 & d_6 & 0 & 2d_3 & d_6\\ 0 & 0 & 0 & d_5 & d_6 & d_3\end{bmatrix}^{-1}\begin{bmatrix}F_1\\ F_3\\ m_4\\ F_5\\ m_6\\ F_7\end{bmatrix} \tag{54}$$

or simply

$$[D] = [K(\omega)]^{-1}_{global} [F] \tag{55}$$

where $[D]$ is the gobal nodal displacement matrix, $[K(\omega)]_{global}$ is the global dynamic stiffness matrix and $[F]$ is the global force matrix.

Now for the case of a submerged tunnel, the wave and current force acting on the structure is in the form of a uniformly distributed force evaluated using Morison's equation or Ogilvie's Classical Solution. As an approximation to this uniformly distributed force, the force can actually be converted to point loads acting at discrete locations along the length of the beam (at the location of discretized nodes used to formulate dynamic stiffness matrix). Once the force is converted to point loads, the displacement along the length of the beam can be easily determined solving equation Eq.(55).

The advantage of using the dynamic stiffness approach is that, unlike modal superpostion method, the eigenvalue analysis is not required before carrying out the forced vibration analysis,. The dynamic stiffness matrix itself contains the mass and stiffness properties of the system.

4. PARAMETRIC INVESTIGATIONS

Based on the mathematical formulations of previous section a parametric study is carried out to understand the effect of different structural parameters and wave parameters on the dynamic properties of tunnel and the resulting structural response due to wave excitation. For the purpose of analysis a submerged circular acrylic tunnel with internal diameter 4m and external diameter 3.5m has been considered, otherwise noted. The properties of acrylic used for analysis have been summarized in Table 5

Table 5 Structural properties of acrylic

Elastic Modulus	3300 MPa
Poisson's Ratio	0.37
Safety Stress Permissible Water Side	3 MPa
Safety Stress Permissible Air Side	5 MPa
Density	1190kg/m^3

4.1. Effect of Tunnel Length on Natural Frequency for Freely Spanning Tunnel

For a fully acrylic tunnel with internal and external diameters as 4m and 3.5m respectively, the change in natural frequency and time period with increasing length of tunnel is shown in Figure 19 and Figure 20. It is evident from figure that the natural frequency decreases with an increase in the tunnel length. This can be attributed to the overall decrease in the stiffness of the system as the tunnel length increases. Subsequently, the time period increases with an increase in the length of the tunnel. Also, the natural frequencies are very closely spaced for longer tunnel lengths due to greater reduction in

natural frequencies for higher modes. This shows that for longer tunnels the effect of higher modes can be significant while evaluating the overall response of the structure.

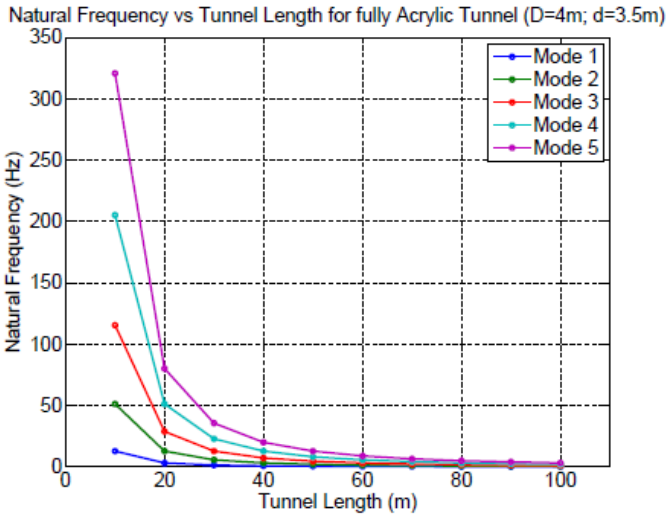

Figure 19 Variation of natural frequency with tunnel length

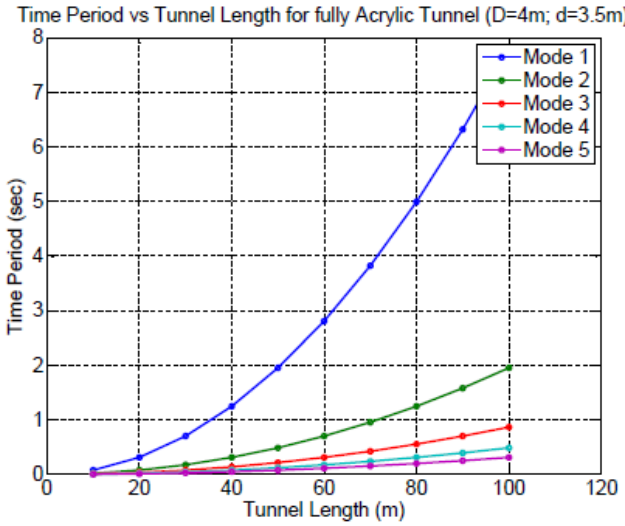

Figure 20 Variation of time period with tunnel length

4.2. Effect of Tether Stiffness and BWR ratio on Natural Frequency

It is evident that the addition of tethers increases the overall stiffness of the system and will lead to increase in the natural frequency of system. Figure 21 shows the variation of first mode frequency of heave motion with increasing tunnel length for different tether stiffness's. From Figure 21 it is clear that the natural frequency of mode 1 increases as the tether stiffness is increased from 0 to 2000kN/m/m. Another important point to note from Figure 21 is that for higher tether stiffness the natural frequency of vibration for first mode becomes constant for tunnel length >50m. This illustrates that tether stiffness greatly controls the lower mode frequencies and can significantly control the overall response of the tunnel.

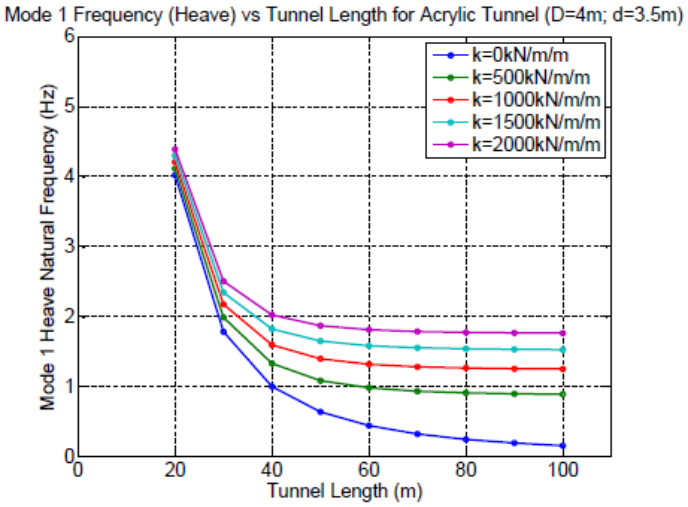

Figure 21 Variation of heave fundamental frequency with tunnel length for different tether stiffness values

For the sway motion of vertically tethered tunnel, it is evident from (4) that tether tension controls the stiffness and the corresponding natural frequencies. The pre-tension

in tethers depends on the buoyancy-to-weight ratio (BWR) of the tunnel. Figure 22 illustrates the effect of BWR on the natural frequencies of sway modes for different tunnel lengths. For L=50m it can be seen that the tunnel natural frequencies is unaffected by the change in BWR. However, as the tunnel length increases (L=100m, L=150m, L=200m) the natural frequencies shows an increasing trend with increasing BWR. This implies that for longer tunnels BWR significantly controls the natural frequencies for sway motion and can be used to control the tunnel response in sway motion.

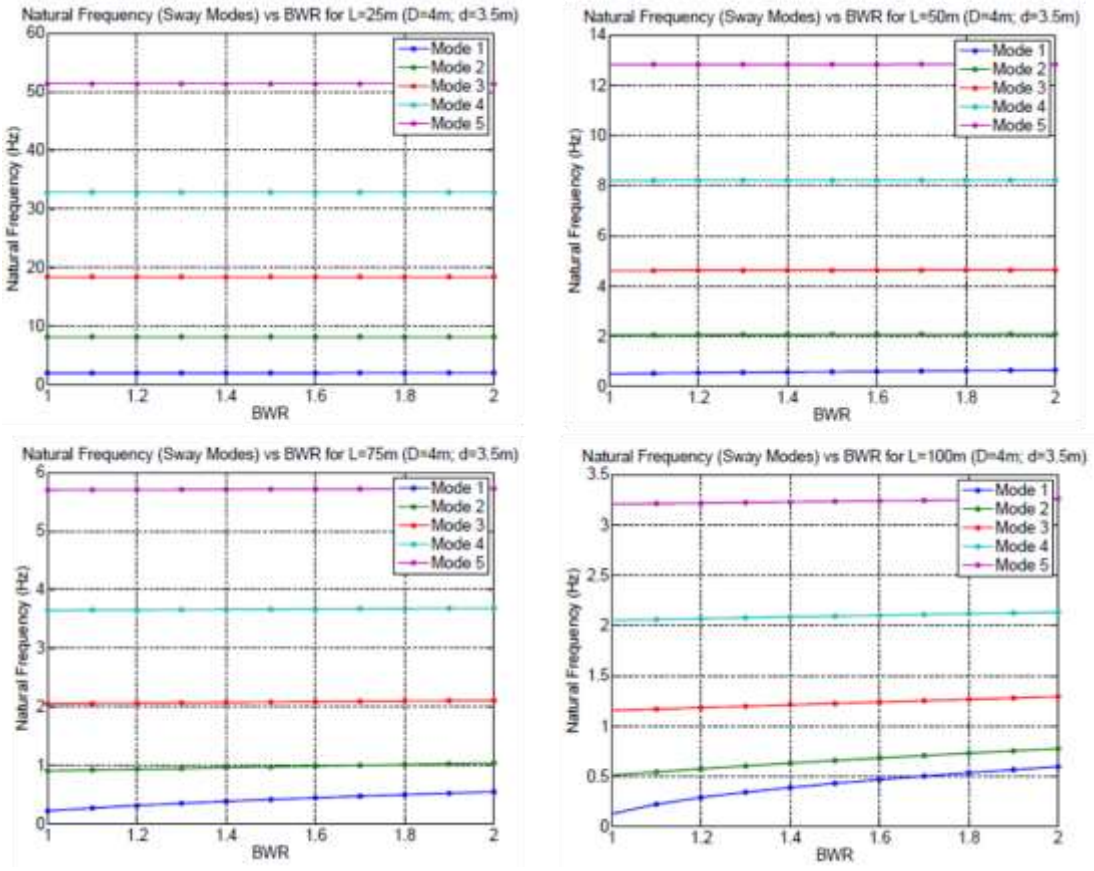

Figure 22 Variation of natural frequency for sway modes for different BWR ratios

4.3. Effect of Tether Inclination on Natural Frequency of Tunnel

For the case when tethers are inclined, the stiffness provided by the tethers has both horizontal and vertical contribution depending on the tether inclination from vertical. This leads to a decrease in the natural frequency for heave modes and a significant increase in the natural frequency for sway modes as shown in Figure 23.

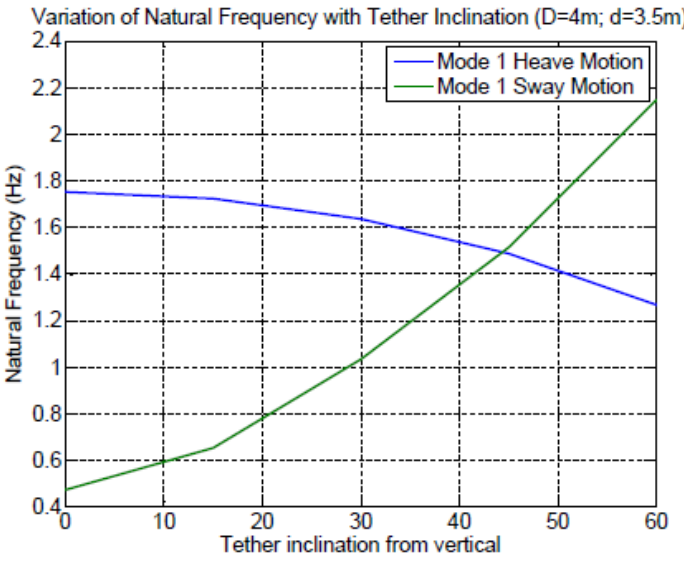

Figure 23 Variation of heave and sway natural frequency with tether inclination

Also, it can be seen from Figure 23 that for tether inclination 45°, the natural frequency for heave and sway modes are equal owing to equal tether stiffness in horizontal and vertical direction.

4.4. Effect of Eccentricity on Sway Frequency for different Tunnel Lengths

For tunnels made of acrylic-steel combination, the effect of eccentricity introduced on the natural frequency of vibration of tunnel is studied. To understand the effect of eccentricity three cases have been considered:

- Tunnel with cross-sectional dimension D=4m d=3.5m
- Tunnel with cross-sectional dimension D=10m d=9m
- Tunnel with cross-sectional dimension D=15m d=14m

For each of the three cases the steel spine extends an arc of 120 degrees at the center of cross-section. For each case the variation of first natural frequency of vibration with increasing eccentricity has been studied for different tunnel lengths (L=25, L=50m, L=100m).

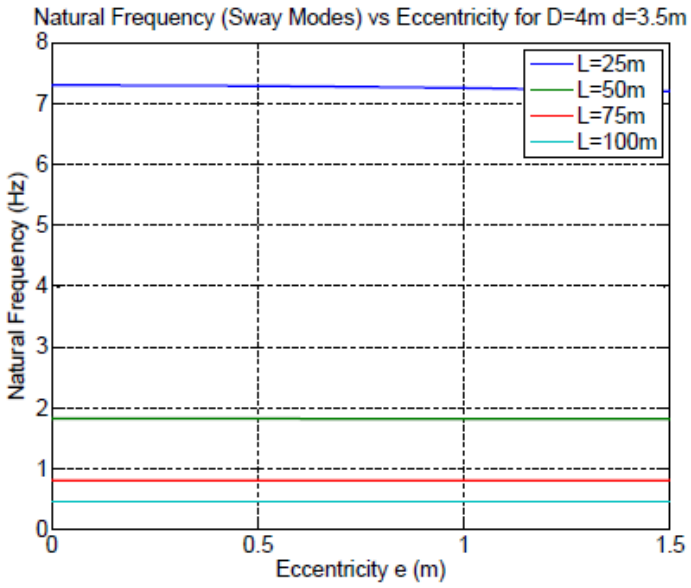

Figure 24 Variation of sway natural frequency with tunnel eccentricty for tunnel with dimension D=4m and d=3.5m

From Figure 24 it can be seen that for longer tunnels the natural frequency remains constant when the tunnel eccentricity is increased. However, for tunnel length L=25m slight reduction in natural frequency is observed with increasing tunnel eccentricity.

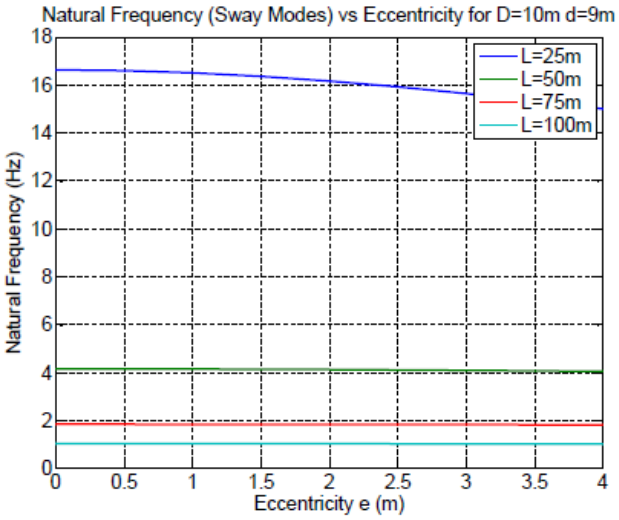

Figure 25 Variation of sway natural frequency with tunnel eccentricty for tunnel with dimension D=10m and d=9m

Figure 25 again shows the same trend as Figure 24. Even for a larger diameter tunnel the natural frequency of vibration of longer tunnels remain unaffected by increasing eccentricity. However, the reduction in natural frequency for smaller tunnel L=25m is found to be significant with increasing eccentricity.

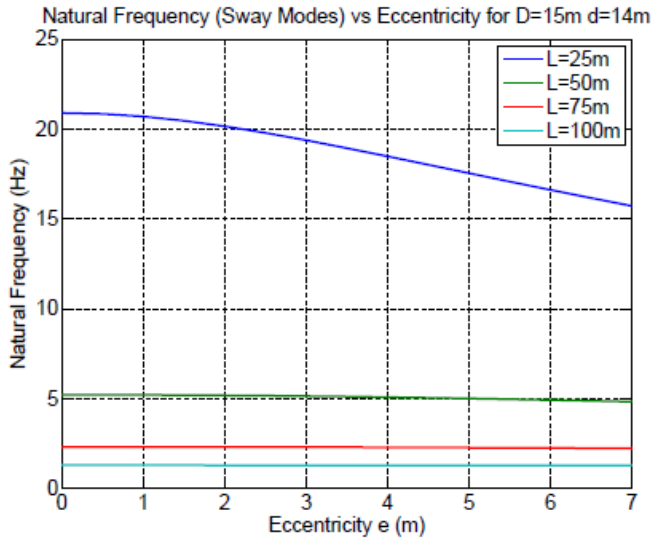

Figure 26 Variation of sway natural frequency with tunnel eccentricty for tunnel with dimension D=15m and d=14m

Figure 26 shows the variation of natural frequency with eccentricity for tunnel with cross-sectional dimensions D=15m d=14m. It is evident from the figure that a significant reduction in natural frequency is observed for tunnel length L=25m. Also, for tunnel length L=50m, a very small reduction in natural frequency is observed. However, for length L=75m and L=100m, once again the natural frequency stays unaffected by tunnel eccentricity.

From the trend shown by curves in Figure 24, Figure 25 and Figure 26 it can be concluded that for longer tunnels (L>50m) the effect of eccentricity on the natural frequency of vibration is negligible and can be ignored. However, for intermediate and smaller tunnels (25m<L<50m), a significant reduction in natural frequency is observed with increasing eccentricity. Also, the reduction is prominent for tunnels with large cross-sectional dimensions.

4.5. Variation in Coupled Mode Shapes with Tunnel Eccentricity and Length

Once the natural frequencies are known, the corresponding mode shapes of vibration are determined Figure 27, Figure 28 and Figure 29 shows the first five mode shapes for an acrylic-steel tunnel with cross-sectional dimensions D=4m and d=3.5m. The mode shapes have been plotted for three different tunnel lengths (L=25m, L=50m and L=100m). From Figure 27 it is evident that for tunnel length 25m, the bending modes dominate for first two modes. But strong coupling between bending and torsional modes can be seen from third mode onwards. However, as the tunnel length increases L=50m and L=100m, it can be seen from Figure 28 and Figure 29 that the coupling reduces significantly even for higher modes. This again shows that the bending modes are dominant for longer tunnels with very small torsional effects.

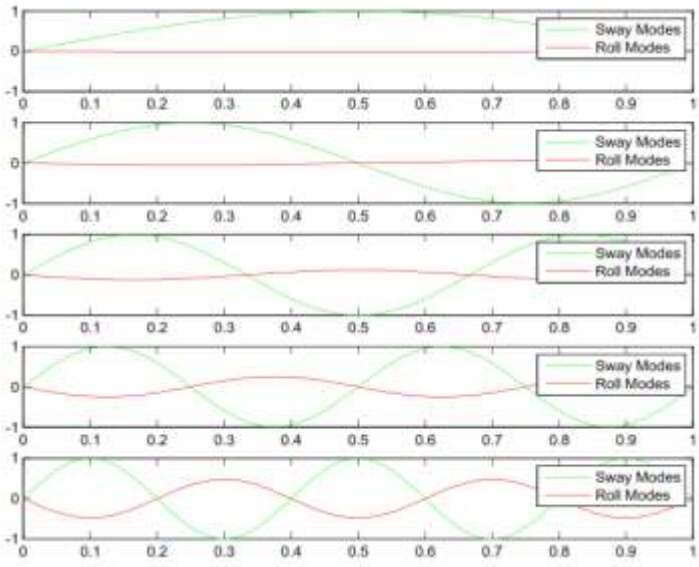

Figure 27 Modes of vibration for tunnel length L=25m

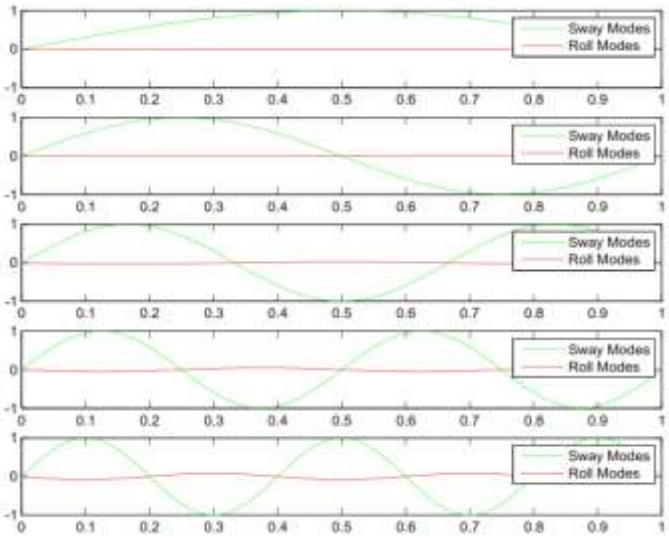

Figure 28 Modes of vibrations for tunnel length L=50m

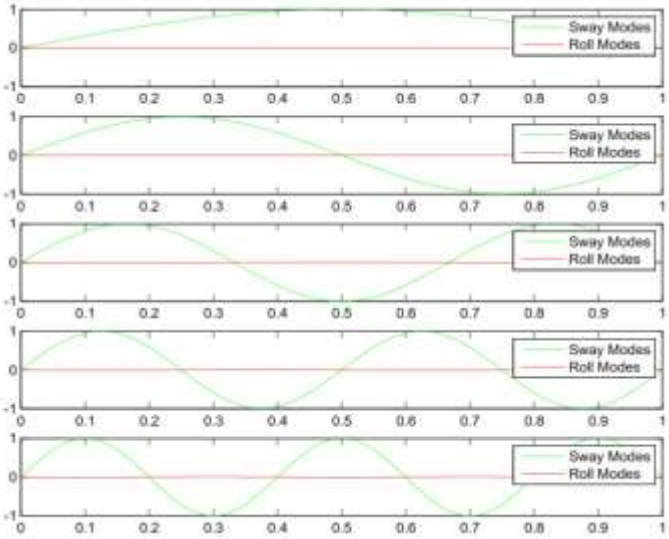

Figure 29 Modes of vibration for tunnel length L=100m

4.6. Variation in Critical Buckling Pressure for Circular Acrylic Tunnels

Using analytical expressions for critical buckling pressure given by different formulas in Section 3.5 a design curve is prepared for critical buckling pressure as a

function of thickness-radius ratio of circular cylinder for a given length-diameter ratio. The design curve can further be used to decide the thickness of acrylic panels for submerged circular cylindrical tunnel cross-sections, effective to resist the hydrostatic pressure at a given depth of submergence.

The critical pressure curves in Figure 30 have been generated for acrylic with safe design stress value of 5 MPa and modulus of elasticity 3300 MPa. From Figure 30 it can be seen that for 5-20m submergence depth of tunnel (0.05-0.2MPa hydrostatic pressure), the design of acrylic panel is governed by critical pressures for failure due to elastic instability of long tubes. Also, it is evident that for large values of L/D ratio the critical pressure approaches the case of long tubes instability pressure.

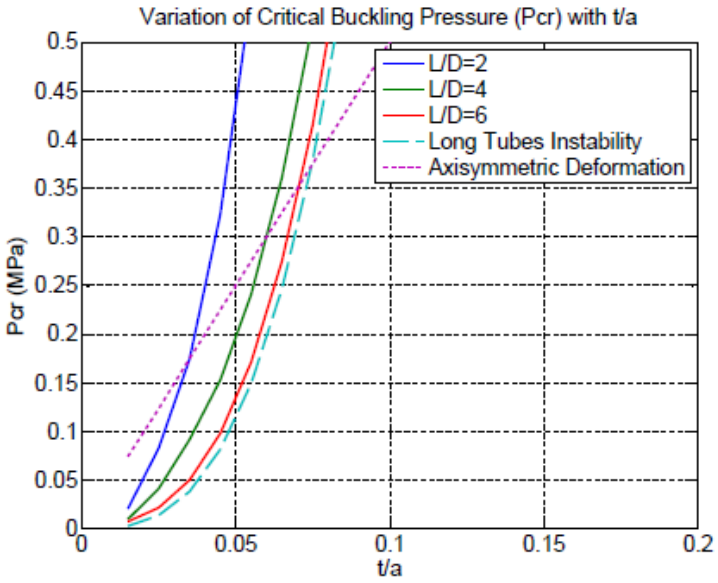

Figure 30 Variation of critical buckling pressure with L/D and t/a ratio for circular tunnels

4.7. Variation in Critical Buckling Pressure with Tunnel Ovality

Figure 31 shows the change in the ratio of critical buckling pressure of cylinders with ellipticity to critical buckling pressure of perfectly circular cylinder with the increase in ovality of the system. From Figure 31 it is evident that with an increase in the ovality of tunnel cross-section, there is an exponential reduction in the critical buckling pressure of tunnel cross-section with respect to that of a perfect circular cylinder. Hence, use of elliptical cross-sections for submerged tunnels is preferable only for cases when the depth of submergence is not very large.

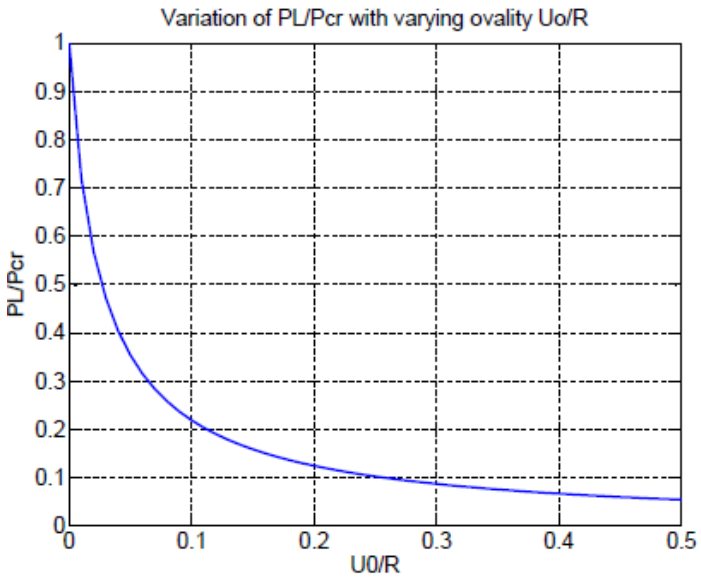

Figure 31 Variation of buckling pressure with increasing tunnel ovality

4.8. Variation in Critical Buckling Pressure for Elliptical Tunnel

For a tunnel cross-section with ovality, the variation of critical buckling pressure with t/a ratio of the tunnel can be seen in Figure 32

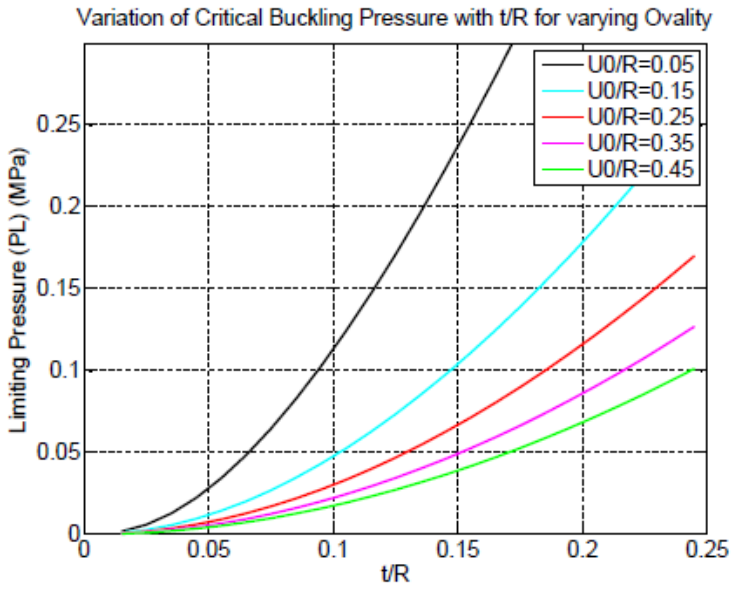

Figure 32 Variation of critical buckling pressure with u_0 / R and t/R ratio for elliptical cross-section tunnels

The design curves of Figure 32 can be used to determine the wall thickness of elliptical cylindrical tunnel sections to be used at a given depth of submergence subjected to external hydrostatic pressure.

4.9. Comparison of Wave Load by Morison's Equation vs Ogilvie's Solution

Using the expression for total force on a submerged circular cylinder formulated in 3.7, force on a submerged circular tunnel has been evaluated and compared to the force given by Morison's Equation with drag coefficient $C_D = 1.2$ and inertia coefficient $C_M = 2.0$ for three depths of submergence of tunnel (z=3m, z=5m, z=10m). The results of the comparison are shown in Figure 33, Figure 34 and Figure 35. For force evaluation

the wave parameters of AB Prototype for Qiandao Lake, China has been used ($H_s = 1m$, $T_p = 2.3\sec$).

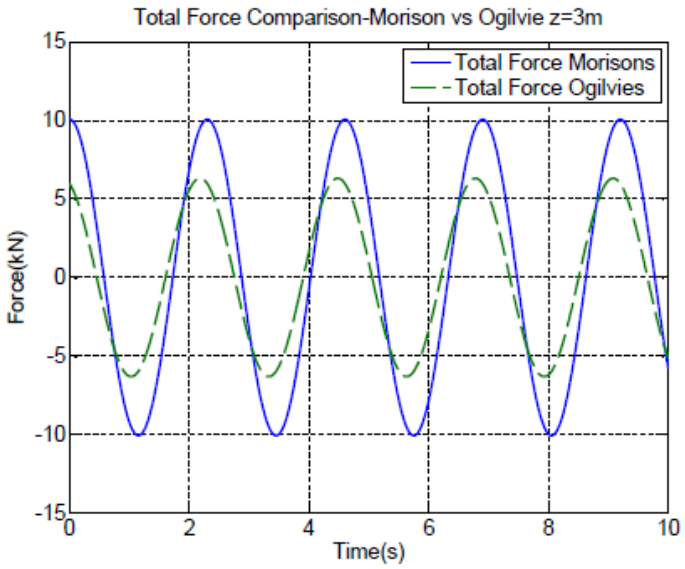

Figure 33 Force comparion Morison's equation vs Ogilvie's solution at z=3m

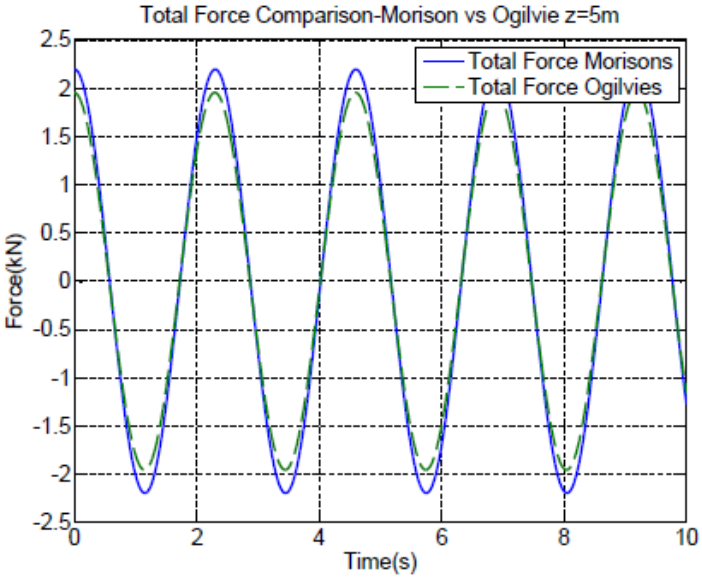

Figure 34 Force comparion Morison's equation vs Ogilvie's solution at z=5m

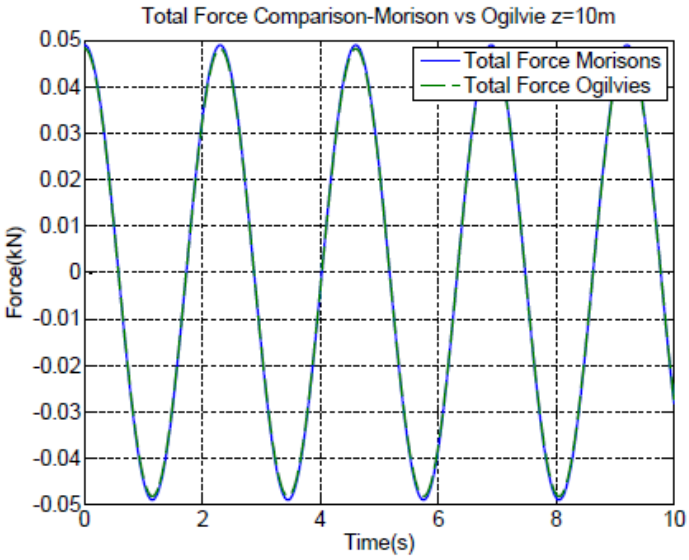

Figure 35 Force comparions Morison's equation vs Ogilvie's solution at z=10m

From Figure 33 it can be seen that for tunnel at depth $z = 3m$ Morison's equation gives a higher value of force than Ogilvie's solution. Since the force given by Ogilvie solution is more exact in nature, it can be concluded that the value of C_M parameter used in Morison's equation is higher and can be adjusted to a lower value. Also, the drag contribution to the total force is very small when compared to inertial contribution. This can be attributed to the fact that the tunnel dimension is large enough that no separation of flow occurs. Furthermore, from Figure 34 and Figure 35 it is evident that as the depth of submergence increases both Morison's equation and Ogilvie's solution converge. The result that both the solutions converge at large water depths can be used to establish the fact that application of Morison's equation for evaluating wave loads on submerged bodies at greater water depths is justified.

4.10. Variation of Wave Force with non-dimensional parameter Kh

Using Ogilvie's solution wave loads curves have been prepared for normalized force $\frac{F}{\rho g L H / 2}$ variation with the non-dimensional parameter Kh for a range of values of non-dimensional parameter Ka (Figure 36 and Figure 37). Based on the wave parameters at tunnel site and preliminary dimensions of tunnel, the curves can be easily used to evaluate the magnitude of wave loads on the tunnel. Also, from Figure 36 and Figure 37 it can be seen that the magnitude of wave force decreases exponentially with the increase in depth from the free surface. This reduction in the magnitude of force is more rapid for the range of Ka parameter less than 1 than for range of Ka greater than 1. For values of ka parameter close to Kh, it can be seen that the curves show a little peak. It is suggested that the left hand part of the curve must be interpreted with care as $Ka \approx Kh$ indicates proximity to the free surface. In fact as suggested by Ogilvie [45], for linear theory to hold the incident wave amplitude must be smaller than the distance between cylinder top and undisturbed free surface.

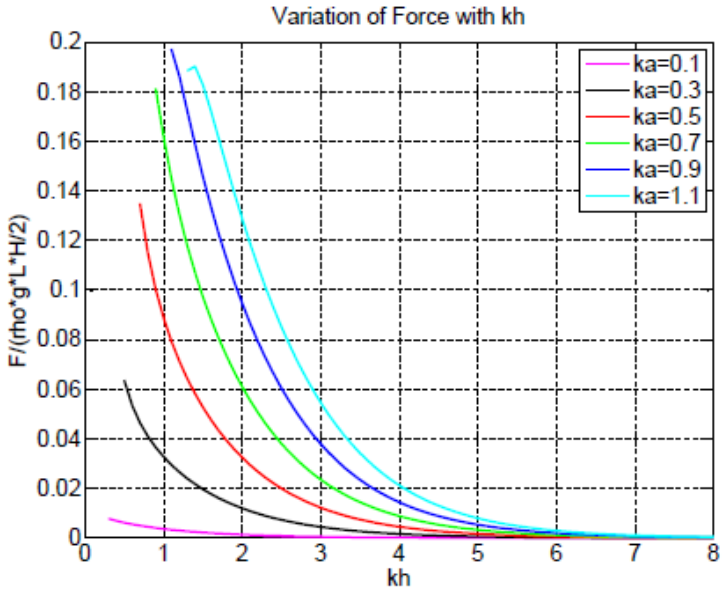

Figure 36 Variation of wave loading with kh for 0.1<ka<1.1

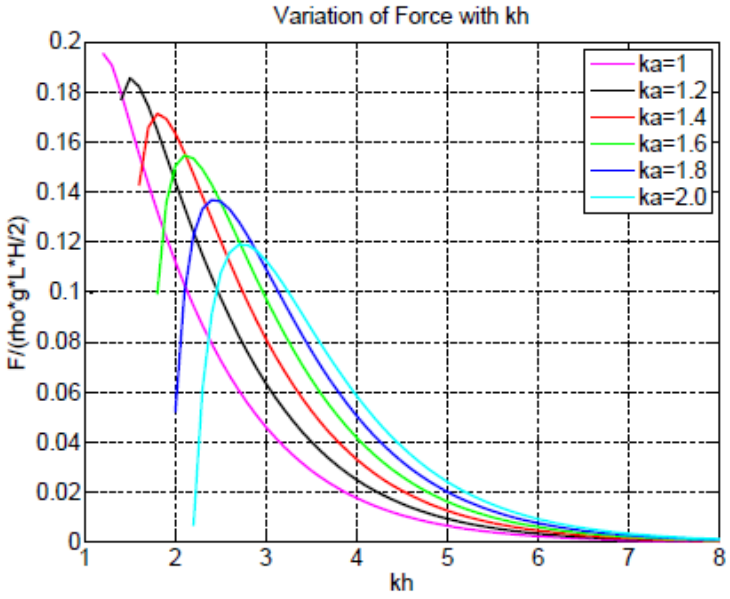

Figure 37 Variation of wave loading with kh for 1<ka<2

4.11. Variation in Wave Load with parameter K (Wave Number)

Figure 38 shows that variation of wave loads with the wave number K for different depth of submergence of floating tunnel. It is evident that the peak value of force decreases with the increase in depth from free surface. Also, the value of wave number parameter K at which the peak occurs shifts to a lower value as the depth of submergence of tunnel increases. This illustrates that not all the waves propagate to deeper water. Waves with low wave number cause peak force at greater water depths.

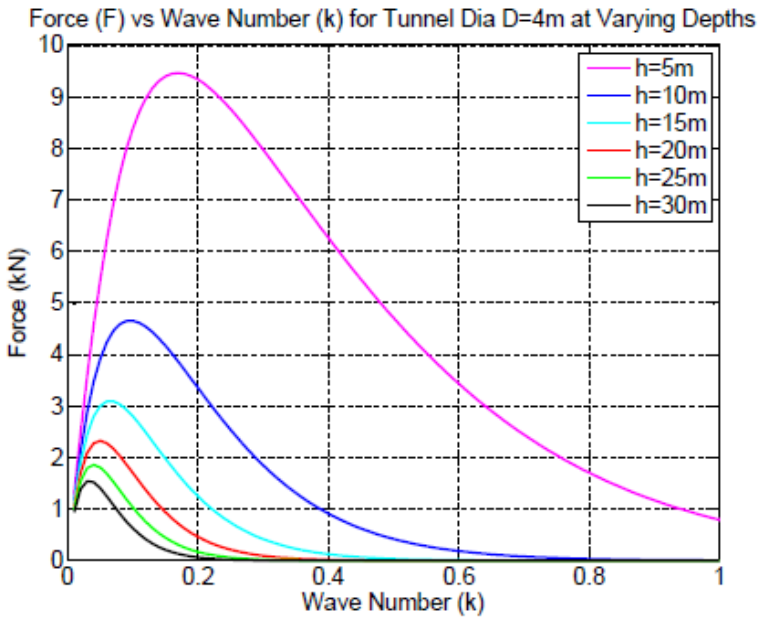

Figure 38 Variation of wave loading with wave number for different water depths

5. NUMERICAL CASE STUDY

For the purpose of numerical simulation the case of Daikokujima Floating Tunnel proposed in Japan is considered. The proposed tunnel will be located at a maximum water depth of 12m. The cross-section of the tunnel has an outer radius of 4m and thickness of 0.3m. In addition, light weight concrete with exterior steel skin plate is considered as a suitable structural material for the proposed tunnel. However, for this study Acrylic and Acrylic-Steel combination is considered as the primary structural material for tunnel.

Using several variations in length and cross-sectional shape of tunnel, the response behavior of tunnel is studied. The design wave conditions for the tunnel are relatively moderate and the main purpose of this tunnel is to serve as pedestrian walkways.

The ends of the tunnel are restrained with two different support conditions. One end of the tunnel is hinged which restrains all translational degrees of freedom and at the other end a roller support is considered which restrains the degrees of freedom in transverse direction and allows only longitudinal and rotational degrees of freedom.

Circular cross-section as shown in Figure 39 is considered for the numerical case study purpose. Using the basic parameters summarized in Table 6 the behavior of different tunnel configurations is discussed in detail in the next few sections.

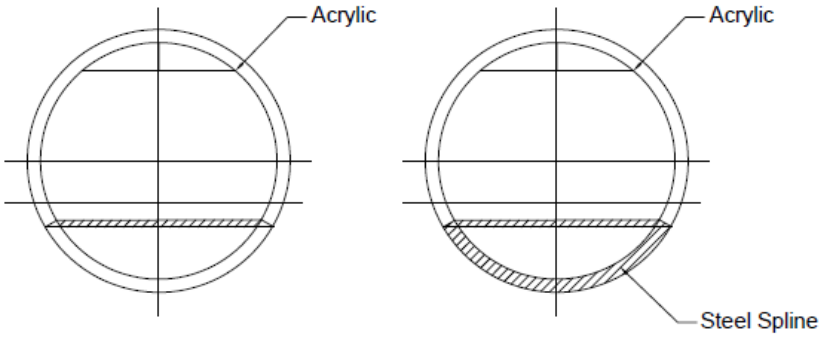

Figure 39 Cross-sectional configurations for numerical case study

Table 6 Summary of base structural parameters

Circular Cross-section			
Parameter	**Unit**	**For Acrylic Only**	**For Acrylic-Steel Combination**
Outer Dia.	m	4	4
Inner Dia.	m	3.4	3.4
Thickness	m	0.3	0.3
Area, A_{cs}	m^2	3.49	3.49
Moment of Inertia, I_{xx} (about x-x)	m^4	6.01	9.72
Moment of Inertia, I_{yy} (about y-y)	m^4	6.01	5.89
Polar Moment of Inertia , I_p	m^4	12.02	15.61
Elastic Modulus Acrylic, E_{acy}	N/m^2	3.30E+09	3.30E+09
Elastic Modulus Steel, E_{st}	N/m^2	2.00E+11	2.00E+11
Flexural Rigidity, EI_{xx}	$N\text{-}m^2$	1.98E+10	1.59E+11
Flexural Rigidity, EI_{yy}	$N\text{-}m^2$	1.98E+10	1.86E+11
Density Acrylic, ρ_{acy}	kg/m^3	1190	1190
Density Steel, ρ_{st}	kg/m^3	7850	7850

5.1. Case-1 10m Long Acrylic Tunnel with Circular Cross-Section

For this case a free spanning straight tunnel with no intermediate supports is analyzed. Under the assumption that the tunnel is located at a water depth of 10m, the maximum hydrostatic pressure acting on the tunnel is evaluated and is equal to 0.1 MPa. To prevent failure under hydrostatic pressure the critical buckling pressure of cross-section should be greater than the maximum hydrostatic pressure. Using formulations of Section-3.5, the critical buckling pressure for each failure mode is determined and given as,

For Failure due to Axisymmetric Yielding, P_{cr} = 0.8 MPa

For Failure due to Elastic Instability, P_{cr} = 1.04 MPa (PKD=6)

It is evident that axisymmetric yielding is the governing failure mode for this case and the critical buckling pressure for yielding is greater than 0.1 MPa. Hence, the cross-sectional shape is safe against hydrostatic pressure.

Using the basic cross-sectional and material properties the mass per unit of the tunnel is determined as $mass/length = \rho_{acy} \times A_{cs}$ and is equal to 4.15×10^3 kg/m. Assuming, a uniform load of 90 psf for pedestrians, the mass per unit length on tunnel due to pedestrian is 1.32×10^3 kg/m which makes the total weight of the tunnel along with pedestrian loading as 5.47×10^3 kg/m. The buoyant force acting per unit length of tunnel depends on the outer diameter of tunnel and is equal to 1.28×10^4 kg/m. Using the weight/per unit length and buoyancy, the buoyancy to weight ratio (BWR) of the tunnel is determined and is equal to 2.35. Since the tunnel is freely spanning the BWR ratio should be equal to 1.0 to ensure stability. Hence, additional ballast maybe required to balance the

self-weight with buoyancy. Taking into account the additional ballast, the equivalent density of acrylic required to balance the buoyant force is calculated as $\rho_{eq} = buoyancy / A_{cs}$ and is equal to 3694 kg/m^3.

Using the equivalent density of acrylic, the effective mass of tunnel is determined and is further used in the evaluation of natural modes of vibration of the tunnel. Apart from effective mass of tunnel, added mass of water is also required in the evaluation of natural modes. For this study the added mass is assumed to be constant for all modes of vibration and is evaluated as,

$$m_{add} = \frac{\pi D^2}{4}\left(C_M - 1\right)$$

where D is the outer diameter of tunnel and C_M is the inertia coefficient equal to 2.0. Now, using the formulations of Section 3.1, the natural period of vibration of tunnel is determined and summarized in Table 7.

Table 7 Natural period of vibration for acrylic tunnel L=10m

Eigenvalue Number	Period (sec)	Frequency (Hz)	Mode of Vibration
1	0.0744	13.44	Heave/Sway
2	0.0186	53.76	Heave/Sway
3	0.0083	120.48	Heave/Sway
4	0.0047	212.77	Heave/Sway
5	0.003	333.33	Heave/Sway

From Table 7 it can be seen that the period of 1st mode of vibration of tunnel is very low and would not lie in the range of excitation due to wave loading. Also, fundamental frequency in vertical mode and horizontal mode is greater than 3Hz and 1.3 Hz respectively. This ensures no excitation due to pedestrian movement over the tunnel. Hence, the dynamic effects on the tunnel would be insignificant in this case. The static loads due to waves would determine the stresses and tunnel displacements.

In Section-4.9 it was shown that wave loads given by Morison's equation and Ogilvie's solution converge at water depths > 5m. For this case since it is assumed that the tunnel is located at a water depth of 10m, hence either of Morison's equation or Ogilvie's solution can be used to get static wave loads. Since the design wave conditions are moderate, a regular wave of height H=1m and period T=2.5 seconds is considered for this case. The design wave conditions are similar to the one used for design of Qiandao Lake SFT prototype. Based on the wave parameters assumed, the resulting static values of drag and inertia horizontal and vertical components of wave load is $w =$ 0.14 kN/m.

Since the tunnel is assumed to be simply supported at the ends, the maximum bending moment acting at the mid span is given by,

$$M = \frac{wl^2}{8} = 1.75kN - m$$

Subsequent bending stress is determined as,

$$\sigma_{\max} = \frac{Mc}{I} = 582N/m^2 = 5.82 \times 10^{-4} MPa$$

The allowable safe stress limit for Acrylic plastic is 5 MPa which is much greater than bending stress value obtained. Hence, the tunnel will be safe against bending due to wave action.

The static displacement of tunnel under wave loads is evaluated as displacement of a simply supported beam under uniformly distributed load and given as

$$u_{static} = \frac{5}{384}\frac{wl^4}{EI} = 9.2\times10^{-7}\,m$$

The static displacement of tunnel is very small and well within the allowable deflection limit L/500 for pedestrian bridges.

The numerical calculations performed for the 10m circular acrylic tunnel shows that the tunnel meets required minimum allowable limits for both strength and serviceability and can be used as a viable underwater pedestrian walkway option.

5.2. Case-2 30m Long Acrylic-Steel Tunnel with Circular Cross-Section

Like previous case, the tunnel is again assumed to be located at a depth of 10m from the free surface. For a 30m long acrylic tunnel the critical buckling pressure for failure due to axisymmetric yielding or elastic instability is again evaluated using formulations of Section-3.5 and given as,

For Failure due to Axisymmetric Yielding, P_{cr} = 0.8 MPa

For Failure due to Elastic Instability, P_{cr} = 1.49 MPa (PKD=2.7)

Axisymmetric yielding is once again the governing failure mode. The evaluated critical buckling pressure is greater than the hydrostatic pressure at 10m water depth. Hence, the

chosen cross-sectional dimension will be safe against hydrostatic pressure for a 30m long tunnel also.

Since the cross-section dimension of tunnel are similar to the previous case the characteristic self-weight of tunnel, pedestrian load and buoyancy will be same as calculated before. These load values are summarized in Table 8. To ensure stability additional ballast would need to be added so that weight per unit length of tunnel becomes equal to buoyant force per unit length.

Table 8 Summary of permanent loads on 30m long acrylic tunnel

Tunnel Self-Weight (kg/m)	4.15×10^3
Pedestrian Load (kg/m)	1.32×10^3
Buoyancy, (kg/m)	1.28×10^4
Buoyancy-weight ratio, BWR	2.34
Equivalent Density Acrylic for BWR=1 (kg/m^3)	3694

Now, using the equivalent density of acrylic and the inertial mass of water the natural modes of vibration of the tunnel is determined and summarized in Table 9.

Table 9 Natural period of vibration for acrylic tunnel L=30m

Eigenvalue Number	Period (sec)	Frequency (Hz)	Mode of Vibration
1	0.6697	1.49	Heave/Sway
2	0.1674	5.97	Heave/Sway
3	0.0744	13.43	Heave/Sway
4	0.0419	23.89	Heave/Sway
5	0.0268	37.33	Heave/Sway

From Table 9 it is evident that although tunnel excitation due to wave induced load may not be significant, but dynamic effects due to pedestrian movement needs to be checked since the fundamental frequency for vertical mode of tunnel is less than 3 Hz and lies in the range of pedestrian excitation frequency. However, this issue can be addressed by increasing the stiffness of tunnel cross-section so that the fundamental frequency for vertical mode becomes greater than 3 Hz.

In order to increase the stiffness of cross-section the tunnel can be stiffened by providing a steel spine at the bottom of cross-section in combination with acrylic. The effect of tunnel stiffening using steel spine is discussed separately in subsequent section.

5.2.1. Acrylic-Steel Combination for Stiffening Tunnel

For stiffening the tunnel a 0.2 m thick steel spine making an angle of 120 degrees at the center of tunnel is used in combination with acrylic at the bottom of cross-section (See Figure 39). Using the basic structural parameters defined in Table 6 for an Acrylic-Steel Tunnel, the characteristic self-weight, pedestrian load and buoyancy per unit length on the tunnel is determined and summarized in Table 10.

Table 10 Summary of permanent loads on 30m long acrylic-steel tunnel

Tunnel Self-Weight (kg/m)	1.05×10^4
Pedestrian Load (kg/m)	1.32×10^3
Buoyancy, kg/m	1.28×10^4
Buoyancy-weight ratio, BWR	1.08
Equivalent Density Acrylic-Steel for BWR=1 (kg/m^3)	3694

Addition of a steel spine to acrylic cross section leads to a significant improvement in the BWR ratio of the tunnel making it more stable. However, the buoyancy-weight ratio is still greater than 1, hence additional ballast is again required to balance the self-weight with buoyant force.

Furthermore, addition of steel spine to the cross-section causes a shift in CG of cross-section towards the steel side. The location of new CG is calculated and found 0.72m below the horizontal axis through centroid of section. Using Roark's Formula for Stress and Strain the flexural rigidity of tunnel cross-section is further evaluated about this new CG. Flexural rigidity of tunnel as calculated are,

About horizontal axis through new CG, $EI_{xx} = 1.59x10^{11}\ m^4$

About vertical axis through new CG, $EI_{yy} = 1.86x10^{11}\ m^4$

Using the calculated flexural rigidities, equivalent density of Acrylic-Steel combination and added mass of water, the natural modes of vibration of tunnel is calculated and compared to those with Acrylic only section. The result of the comparison is summarized in Table 11.

Table 11 Comparison of natural modes for acrylic only and acrylic-steel combination for tunnel with L=30m

	Acrylic Only			Acrylic-Steel Combination		
Eigenvalue Number	Period (sec)	frequency (Hz)	Mode of Vibration	Period (sec)	frequency (Hz)	Mode of Vibration
1	0.670	1.49	Heave	0.230	4.35	Heave
2	0.670	1.49	Sway	0.210	4.76	Sway

Table 11 Continued

	Acrylic Only			Acrylic-Steel Combination		
Eigenvalue Number	Period (sec)	frequency (Hz)	Mode of Vibration	Period (sec)	frequency (Hz)	Mode of Vibration
3	0.167	5.97	Heave	0.057	17.54	Heave
4	0.167	5.97	Sway	0.053	18.87	Sway
5	0.074	13.44	Heave	0.026	39.06	Heave
6	0.074	13.44	Sway	0.024	42.19	Sway
7	0.042	23.87	Heave	0.014	69.44	Heave
8	0.042	23.87	Sway	0.013	75.19	Sway
9	0.027	37.31	Heave	0.009	108.70	Heave
10	0.027	37.31	Sway	0.009	117.65	Sway

An important point to be noted in natural frequency calculation of Acrylic-Steel section is that effect of CG shift or eccentricity is neglected. This stems from the parametric study done in Section-4.4 where it was shown that for intermediate tunnel lengths (25m<L<50m) a very small change in natural frequency is observed for eccentricity range of 0.5m-1.0m.

It is evident from Table 11 that addition of steel spine leads to significant stiffening of cross-section as the natural frequency for first vertical and horizontal mode increases from 1.49 Hz to 4.35 Hz and 4.76 Hz respectively. Now, the fundamental frequency for both horizontal and vertical mode lies well outside the range of excitation by pedestrian movement. Furthermore, taking into account only the excitation due to wave loading the response of the tunnel under a regular wave of height H=1m and period T_p=2.5 sec is

determined using the formulations of Section-3.8. The dynamic response is shown in Figure 40.

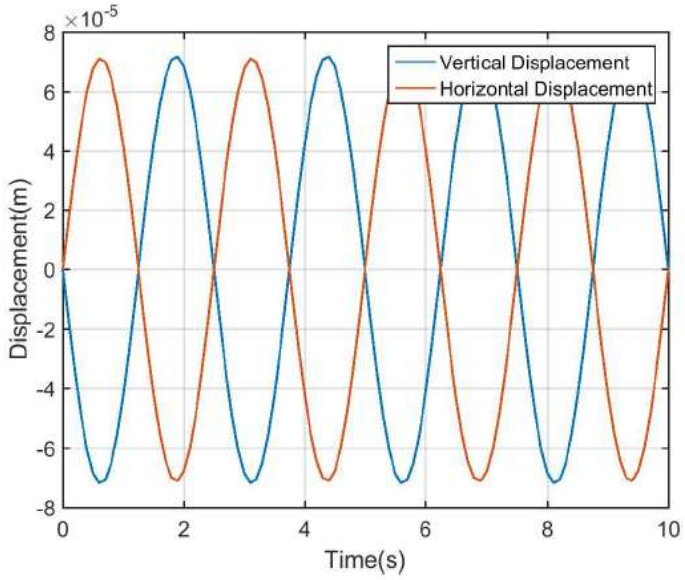

Figure 40 Vertical and horizontal displacement of 30m long acrylic-steel tunnel under regular wave H=1m and T_p=2.5sec

From Figure 40 it can been seen that the mid-span displacement of tunnel is very small and lies in the range of 10^{-5} m. The tunnel thus meets the required serviceability limits of L/500 for pedestrian bridges. Also, the horizontal and vertical displacements are of the same order but they are 180 degrees out of phase with each other. This is attributed to the nature of wave loading in horizontal and vertical direction.

From the numerical simulation results of a 30m long tunnel it is concluded that the use of acrylic-steel combination provides the necessary stiffness to the cross-section leading to substantial reduction in the dynamic effects due to pedestrian movement as well

as wave excitation. The steel spine also leads to improvement in the BWR ratio which is important from stability point of view. Acrylic-Steel tunnel thus presents a viable structural option for pedestrian walkways of intermediate lengths.

5.3. Case-3 50m Long Acrylic-Steel Tunnel with Circular Cross-Section

For a 50m long tunnel, the weight per unit length of tunnel along with pedestrian loading and the buoyant force will be same as that summarized in Table 10 for acrylic-steel as primary structural material. As concluded in the previous case, use of acrylic-steel combination mitigated the vibration issues due to pedestrian movement. Hence, for a 50m long tunnel once again acrylic in combination with steel would be used as the tunnel structural material. The behavior of tunnel under hydrostatic pressure is similar to that of 30m tunnel case as both of them fall under the category of long tubes. Axisymmetric yielding governs the failure mode and the critical buckling pressure for tunnel is 0.8 MPa, which is greater than the maximum hydrostatic pressure of 0.1 MPa at 10m of water depth. Hence, the cross-section is safe against failure under hydrostatic pressure.

Once again using the characteristic weights summarized in Table 10, flexural rigidities calculated in previous case and the added mass of water the natural modes of vibration of the tunnel is evaluated and is reported in Table 12.

Table 12 Natural period of vibration for acrylic-steel tunnel L=50m

Eigenvalue Number	Period (sec)	Frequency (Hz)	Mode of Vibration
1	0.6393	1.56	Heave
2	0.5923	1.68	Sway
3	0.1598	6.25	Heave

Table 12 Continued

Eigenvalue Number	Period (sec)	Frequency (Hz)	Mode of Vibration
4	0.1481	6.75	Sway
5	0.0710	14.08	Heave
6	0.0658	15.19	Sway
7	0.0400	25	Heave
8	0.0370	27.03	Sway
9	0.0256	39.06	Heave
10	0.0237	42.19	Sway

For natural period values calculated in Table 12, the effect of CG shift is not taken into account. This is because it has already been shown through the parametric investigation in Section-4.4 that shift in CG has little effect on natural periods for longer tunnels.

On observing the natural frequency value reported in Table 12, it is found that the fundamental frequency for the vertical mode falls below 3Hz even after tunnel stiffening using a steel spine. The tunnel may be subjected to pedestrian induced vibrations. Hence, additional measures are required to increase the overall stiffness of the system. Further stiffening of the tunnel is done by using vertical tethers which anchor the tunnel to the seabed. The cross-sectional properties of vertical tethers depend on the buoyancy-to-weight ratio of tunnel as the net buoyant force acting on the tunnel is taken by tethers as tension. For tunnel cross-section under consideration, the BWR ratio calculated excluding the pedestrian load is 1.22.

Assuming that the tunnel is anchored by $n_t = 2$ tethers and the tethers are equally spaced, the net tensile force carried by each tether can be determined

$$Tension/tether = \frac{(BWR-1)\times L\times g\times m_t}{n_t}$$

where L is the length of tunnel, g is the acceleration due to gravity, m_t is the total weight of tunnel with pedestrian load.

Tension per tether as determined from equation above is 5.83×10^5 N. Assuming a safe allowable stress value of 70 N/mm^2 for each tether, the required area of cross-section for each tether is 0.0083 m^2. Based on the required area of cross-section of tether and the length of each tether, the available stiffness for tunnel displacement in horizontal and vertical direction is determined as per Section-3.1.

Stiffness for Sway Motion of Tunnel, $K_x = \frac{2T_o}{L_t} = 2.92\times10^5 N/m$

Stiffness for Heave Motion of Tunnel, $K_z = \frac{2AE}{L_t} = 8.33\times10^8 N/m$

Once the tether stiffness is determined, the natural period of vibration of tunnel is evaluated taking into account tether stiffness and compared to the periods for case when no tethers were used. The results of the comparison are summarized in Table 13.

Table 13 Comparison of natural modes for 50m long free spaning and tethered tunnel

	Acrylic-Steel Tunnel No Tethers			Acrylic-Steel Tunnel With Tethers		
Eigenvalue Number	Period (sec)	frequency (Hz)	Mode of Vibration	Period (sec)	frequency (Hz)	Mode of Vibration
1	0.6393	1.56	Heave	0.5626	1.77	Sway
2	0.5923	1.68	Sway	0.1410	7.09	Sway
3	0.1598	6.25	Heave	0.1326	7.54	Heave
4	0.1481	6.75	Sway	0.1014	9.86	Heave
5	0.0710	14.08	Heave	0.0627	15.94	Sway
6	0.0658	15.19	Sway	0.0606	16.50	Heave
7	0.0400	25	Heave	0.0367	27.24	Heave
8	0.0370	27.03	Sway	0.0353	28.32	Sway
9	0.0256	39.06	Heave	0.0240	41.66	Heave
10	0.0237	42.19	Sway	0.0226	44.24	Sway

On comparing the natural frequency values it is observed that addition of vertical tethers results in significant increase in the stiffness for heave motion, as the fundamental frequency value for heave mode jumps from 1.56 Hz to 7.54 Hz. For the sway motion the effect of tether addition is not so significant owing to small increase in the fundamental frequency for sway modes. The fundamental frequency for the sway mode can be increased by using inclined tethers with 45 degree inclination giving equal stiffness in both horizontal and vertical direction.

For this case, however, the issue of pedestrian induced vibration due to fundamental frequency for vertical mode falling below 3 Hz has been resolved by addition of vertical tethers. Now, once the issue of pedestrian vibration is resolved, only the

dynamic effects due to wave excitation needs to be accounted for evaluating the response. In line with this the response analysis of tunnel under a regular wave of height H=1m and period T_p=2.5sec is carried out. Figure 41 shows the vertical and horizontal displacement of the mid-span of tunnel under the regular wave. The figure shows a significant reduction in response in the vertical direction due to the addition of tethers. However, the reduction is very slight in horizontal direction. This is attributed to the fact that the stiffness due to vertical tethers is very small in horizontal direction as compared to the vertical direction.

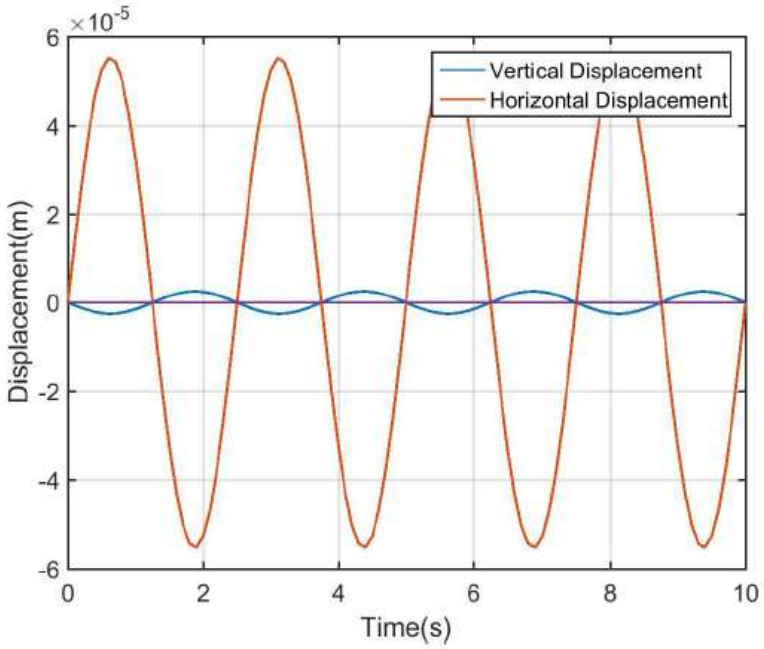

Figure 41 Vertical and horizontal displacement of 50m long tethered acrylic-steel tunnel under regular wave H=1m and Tp=2.5sec

The response behavior shown in Figure 41 is evaluated using the modal superposition approach applied to beam resting on continuous elastic foundation. A more realistic simulation of the tethered tunnel is carried out using the dynamic stiffness model

which treats the tunnel as a beam resting on discrete elastic supports. Figure 42 and Figure 43 presents a comparison of vertical and horizontal displacement of tunnel computed using modal superposition and dynamic stiffness approach. It is evident from figure that displacement values obtained using both approaches are in good agreement with each other.

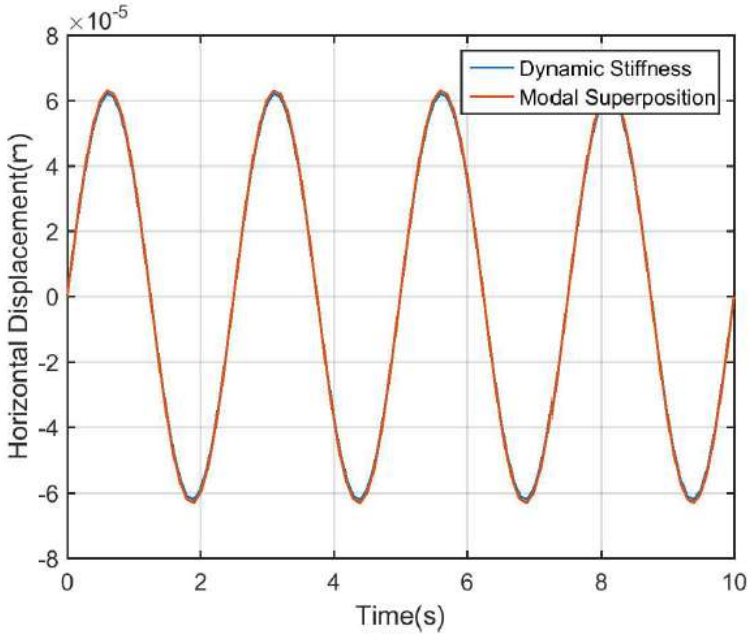

Figure 42 Comparison of mid-span horizontal displacement for tethered tunnel evaluated using modal superposition approach and dynamic stiffness approach

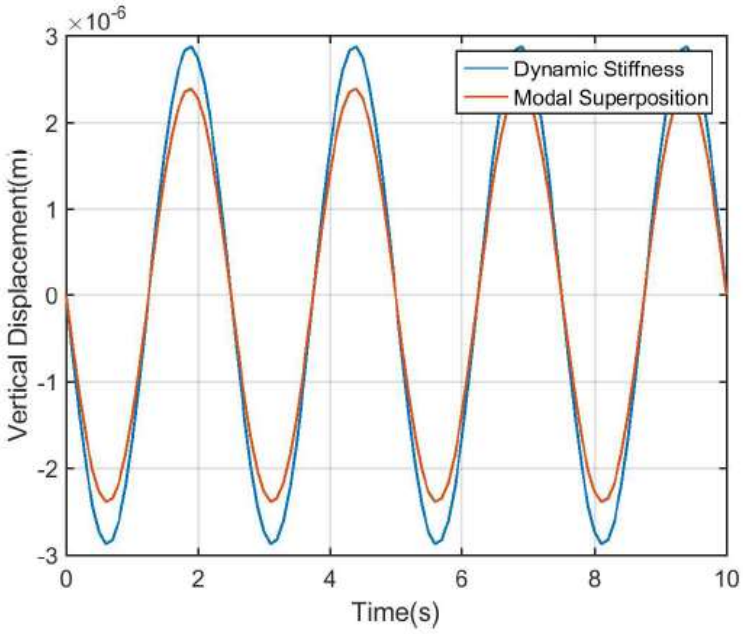

Figure 43 Comparison of mid-span vertical displacement for tethered tunnel evaluated using modal superposition approach and dynamic stiffness approach

6. SUMMARY AND CONCLUSION

To promote underwater tourism and recreational activities around the world a new category of submerged transparent tunnels is proposed in this study. The research study focused on the development of floating and fixed bottom concepts for these submerged tunnels. Assuming the tunnel behavior as an Euler-Bernoulli beam, different structural idealizations of the tunnel were created and subsequent dynamic behavior studied through pure bending and coupled bending-torsion models.

The research also focused on the viability of using acrylic plastic in combination with a steel spine as the primary structural material for tunnel. Based on theoretical buckling pressure models for circular and elliptical cross-sections under external pressure, design charts have been prepared to understand the behavior of acrylic plastic under hydrostatic pressure for different cross-section dimensions. The results of the design charts showed that making the cross-section more elliptical leads to a drastic decrease in the buckling capacity of the cross-section.

The hydrodynamic force resulting from ocean surface waves will be the primary external load on a submerged tunnel. Therefore, this research study examined the disturbance of the incident wave field by considering the importance of diffraction effects. To this end Ogilvie's Classical Solution is used for evaluation of loads on the structure due to surface waves. The results given by Ogilvie's solution were further compared with force computed using Morison's equation to understand the efficacy of Morison's force. The comparison showed that both Morison's and Ogilvie's force converge at greater water

depths and hence Morison's equation can be effectively put to use for tunnel submerged at greater depths. In addition, parametric investigations done showed the variation of global loads with varying tunnel depth and wave parameters.

Combining structural and hydrodynamic models the response behavior of tunnel was studied using purely analytical Modal Superposition approach and analytical/numerical Dynamic Stiffness Approach. Parametric investigations were also carried out to understand how variation in different structural parameters like tunnel length, tether stiffness, buoyancy-weight ratio and tunnel eccentricity affect the modal properties of tunnel. The results of the parametric investigation were helpful in understanding the effect of key structural properties regarding the tunnel response in the numerical case studies considered. The numerical studies demonstrated a step by step approach necessary for the design of submerged tunnels. Moreover, the numerical case studies showed the suitability of different tunnel concepts based on site specific conditions and serviceability requirements.

This research focused on first principles for understanding the behavior of submerged tunnels with transparent acrylic plastic as the primary structural material, which was supported by a steel spine. The result of the study demonstrates the feasibility of this concept from the viewpoint of pedestrian application and aquatourism. However, with the increase in complexity of structural system necessary for actual tunnel designs more advanced finite element models would be required. These complexities may include consideration for tunnel curvature or use of better composite materials in place of steel spine. In addition, hydrodynamic models accounting for non-linear wave excitation and

stochastic load combination procedures can be used to get better estimate of global loads on the structure. Moreover, state-of-the-art CFD tools can be used to get better visualization of flow around the tunnel which will be helpful in developing more optimized and cost-effective tunnel designs.

REFERENCES

[1] Bitterman, N., *'Aquatourism': submerged tourism, a developing area.* Current Issues in Toursim, 2013. **17**(9): p. 772-782.

[2] Murphy, M.J. *Acrylic Tunnels*. 2007; Available from: http://www.mjmurphy.co.nz/ProductsServices/AcrylicTunnels/tabid/304/language/en-US/Default.aspx.

[3] Kanie, S., *Feasibility Study on various SFT in Japan and their technological evaluation.* Procedia Engineering, 2010. **4**: p. 13-20.

[4] Østlid, H., *When is SFT competitive?* Procedia Engineering, 2010. **4**(2010): p. 3-11.

[5] Skorpa, L., *Developing new methods to cross wide and deep Norwegian fjords.* Procedia Engineering, 2010. **4**(2010): p. 81-89.

[6] Jakobsen, B., *Design of the Submerged Floating Tunnel operation under various conditions.* Procedia Engineering, 2010. **4**: p. 71-79.

[7] Tveit, P., *Submerged floating tunnels (SFTs) for Norwegian fjords.* Procedia Engineering, 2010. **4**(2010): p. 135-143.

[8] Mazzolani, F.M., B. Faggiano, and G. Martire, *Design aspects of the AB prototype in the Qiandao Lake.* Procedia Engineering, 2010. **4**: p. 21-33.

[9] Brancaleoni, F., A. Castellani, and P.D. Asdia, *The response of submerged tunnels to their environment.* Engineering Structures, 1989. **11**(1): p. 47-56.

[10] Remseth, S., et al., *Dynamic response and fluid/structure interaction of submerged floating tunnels.* Computer and Structures, 1999. **72**(1999): p. 659-685.

[11] Perotti, F., G. Barbella, and M.D. Pilato, *The dynamic behaviour of Archimede's Bridges: Numerical simulation and design implications.* Procedia Engineering, 2010. **4**(2010): p. 91-98.

[12] Pilato, M.D., F. Perotti, and P. Fogazzi, *3D dynamic response of submerged floating tunnels under seismic and hydrodynamic excitation.* Engineering Structures, 2008. **30**(2008): p. 268-281.

[13] Paik, B.I.Y., et al., *Analysis of wave force induced dynamic response of submerged floating tunnel.* KSCE Journal of Civil Engineering, 2004. **8**(5): p. 543-549.

[14] Ge, F., et al., *Fluid-Structure interaction of submerged floating tunnel in wave field.* Procedia Engineering, 2010. **4**: p. 263-271.

[15] Kunisu, H., et al. *Study on Submerged Floating Tunnel Characteristics Under the Wave Condition*. in *Proceedings of the Fourth International Offshore and Polar Engineering Conference*. 1994. Osaka, Japan.

[16] Long, X., et al., *Effect of fundamental structure parameters on dynamic responses of submerged floating tunnel under hydrodynamic loads.* Acta Mechanica Sinica, 2008. **25**: p. 335-344.

[17] Sato, M., S. Kanie, and T. Mikami, *Structural modeling of beams on elastic foundation with elasticity couplings.* Mechanics Research Communications, 2007. **34**(2007): p. 451-459.

[18] Sato, M., S. Kanie, and T. Mikami, *Mathematical analogy of a beam on elastic supports as a beam on elastic foundation.* Applied Mathematical Modelling, 2008. **32**(2008): p. 688-699.

[19] Tariverdilo, S., et al., *Vibration of submerged floating tunnels due to movind loads.* Applied Mathematical Modelling, 2011. **35**(2011): p. 5413-5425.

[20] Man-sheng, D., et al., *Dynamic equations for curved submerged floating tunnel.* Applied Mathematics and Mechanics, 2007. **28**(10): p. 1299-1308.

[21] Fleischer, D. and S.K. Park, *Plane hydroelastic beam vibrations due to uniformly moving one axle vehicle.* Journal of Sound and Vibration, 2004. **273**: p. 585-606.

[22] Jun, Z., et al., *Analytical Models of Floating Bridges Subjected By Moving Loads for Different Water Depths.* Journal of Hydrodynamics, 2009. **20**(5): p. 537-546.

[23] Newman, J.N., *Wave effects on deformable bodies.* Applied Ocean Research, 1994. **16**(1994): p. 47-59.

[24] Ross, C.T.F., *Pressure Vessels External Pressure Technology*. 2001: Horwood Publishing Chichester.

[25] Hydrosight. *Shapes of Aquarium Tunnels*. 2003 [cited 2015 17th April]; Available from: http://www.hydrosight.com/shapes-of-aquarium-tunnels/.

[26] Stachiw, J.D., *Handbook of Acrylics for Submersibles Hyperbaric Chambers and Aquaria*. 2003: Best Publishish Company.

[27] Stachiw, J.D., *Acrylic plastic as structural material for underwater vehicles.* International Symposium on Underwater Technology, 2004: p. 289-296.

[28] Hydrosight. *Acrylic Panel Thickness*. 2003 [cited 2015 17th April]; Available from: http://www.hydrosight.com/acrylic-panel-thickness/.

[29] Clough, R.W. and J. Penzien, *Dynamics of Structures*. 2003, Berkley, CA: Computers & Structures, Inc.

[30] Martire, G., *The Development od Submerged Floating Tunnels as an Innovative Solution for Waterway Crossing*. 2010, Universita' degli Studi di Napoli Federico II.

[31] Rao, S.S., *Vibrations of Continuous Systems*. 2007: John Wiley & Sons,Inc.

[32] Hosking, R.J., S.A. Husain, and F. Milinazzo, *Natural flexural virations of a continuous beam on discrete elastic supports.* Journal of Sound and Vibration, 2004. **272**(2004): p. 169-185.

[33] Lin, Y.K., *Free Vibrations of A Continuous Beam on Elastic Supports.* International Journal of Mechanical Sciences, 1962. **4**: p. 400-423.

[34] Luo, Y., *Frequency Analysis of Infinite Continuous Beam Under Axial Loads.* Journal of Sound and Vibration, 1997. **213**(5): p. 791-800.

[35] Maurizi, M.J. and D.V.B.D. Rossit, *Free Vibration of A Clamped-Clamped Beam With An Intermediate Elastic Support.* Journal of Sound and Vibration, 1987. **119**(1): p. 173-176.

[36] Rao, K., *Frequency Analysis of Clamped-Clamped Uniform Beams with Intermediate Elastic Support.* Journal of Sound and Vibration, 1989. **133**(3): p. 502-509.

[37] Banerjee, J.R., *Dynamic Stiffness Formulation for Structural Elements: A General Approach.* Computers and Structures 1997. **63**(1): p. 101-103.

[38] Banerjee, J.R., *Free vibration of beams carrying spring-mass systems-A dynamic stiffness approach.* Computer and Structures, 2012. **104-105**: p. 21-26.

[39] Clough, R.W. and J. Penzien, *Dynamics of Structures*. 1975: McGraw-Hill Kogakusha.

[40] Wittrick, W.H. and F.W. Williams, *A General Algorithm for Computing Natural Frequencies of Elastic Structures.* The Quarterly Journal of Mechanics and Applied Mathematics, 1971. **24**(3): p. 262-284.

[41] Bryan, G.H. *Application of the Energy Test to the Collapse of a Long Thin Pipe Under External Pressure*. in *Cambridge Philosophical Society Proceedings*. 1888.

[42] Southwell, R.V., *On the Collapse of Tubes by External Pressure.* Philosophical Magazine Series 6, 1913. **26**(153).

[43] Windenburg, D.F. and C. Trilling, *Collapse by Instability of Thin Cylindrical Shells Under External Pressure.* ASME, 1934. **11**: p. 819-825.

[44] Timoshenko, S., *Strength of Materials Part II Advanced Theory and Problems*. Third Edition ed. 1956.

[45] Ogilvie, T.F., *First- and second-order forces on a cylinder submerged under a fre surface.* Journal of Fluid Mechanics, 1963. **16**: p. 451-472.

[46] Arena, F., *Interaction between long-crested random waves and a submerged horizontal cylinder.* Physics of fluids, 2006. **18**.

APPENDIX-A

Solution of Governing Equation for Pure Bending Behavior of Euler-Bernoulli Beam

The governing partial differential equation for a Free Spanning Floating tunnel idealized as a simply supported Euler-Bernoulli beam is given by [29]

$$EI\frac{\partial^4 v(x,t)}{\partial x^4}+m\frac{\partial^2 v(x,t)}{\partial t^2}=F(x,t) \tag{56}$$

In order to understand the dynamic response behavior of the structure it is necessary to carry out the eigenvalue analysis and determine the natural frequencies of structure. For the free vibration analysis the excitation term in the right side of Eq.(56) is equated to zero. Using the method of separation of variables the governing partial differential equation is further reduced into two separate ordinary differential equations in space and time.

The solution $v(x,t)$ can be assumed of the form

$$v(x,t)=\Phi_n(x)V_n(t) \tag{57}$$

Substituting Eq.(57) into Eq.(56) gives

$$EI\Phi_n{}''''(x)\mathrm{V}_n(t)=-\mathrm{m}\,\Phi_n(x)\ddot{\mathrm{V}}_n(t) \tag{58}$$

which leads to

$$\frac{EI\Phi_n{}''''(x)}{m\Phi_n(x)}=-\frac{\ddot{V}_n(t)}{V_n(t)}=\omega_n{}^2 \tag{59}$$

where ω_n is a constant

Eq.(59) can be further written as two separate equations as

$$\ddot{V}_n(t) + \omega_n^2 V_n(t) = 0 \tag{60}$$

$$EI\Phi_n''''(x) - m\omega_n^2 \Phi_n(x) = 0 \tag{61}$$

The solution of Eq.(60) and Eq.(61) is given as

$$V_n(t) = A\sin(\omega_n t - \beta_n) \tag{62}$$

$$\Phi_n(x) = B_1\cosh(\alpha_n x) + B_2\sinh(\alpha_n x) + B_3\cos(\alpha_n x) + B_4\sin(\alpha_n x) \tag{63}$$

where

$$\alpha_n^4 = \frac{m\omega_n^2}{EI}$$

Eq.(63) has four constants which can be determined using the specified boundary conditions of the tunnel. For our case the tunnel has been considered as simple supported at the end supports and the boundary conditions are given as

$$\text{At } x = 0 \qquad \Phi_n(x) = 0$$

$$EI\Phi_n''(x) = 0$$

$$\text{At } x = L \qquad \Phi_n(x) = 0$$

$$EI\Phi_n''(x) = 0$$

On applying the given boundary conditions to Eq.(63) we get

$$B_4\sin(\alpha_n L) = 0 \tag{64}$$

For non-trivial solutions of Eq.(64)

$$\sin(\alpha_n L) = 0$$

$$\alpha_n = \frac{n\pi}{L} \tag{65}$$

which gives

$$\frac{m\omega_n^2}{EI} = \left(\frac{n\pi}{L}\right)^4$$

$$\omega_n = \sqrt{\left(\frac{n\pi}{L}\right)^4 \frac{EI}{m}} \tag{66}$$

Eq.(66) gives the natural frequency of vibration of a freely spanning straight tunnel under the assumption that the shore connections are simply supported. The mode shapes of vibration of the tunnel is given by

$$\Phi_n(x) = B_4 \sin\left(\frac{n\pi x}{L}\right) \tag{67}$$

Using the property of orthogonality of normal modes the nth normal mode can be normalized as

$$\int_0^L m\Phi_n^2(x)\,dx = 1 \tag{68}$$

Substituting Eq.(67) in Eq.(68) and solving for B_4 we get

$$B_4 = \sqrt{\frac{2}{mL}} \tag{69}$$

The normal modes of vibration can then be written as

$$\Phi_n(x) = \sqrt{\frac{2}{mL}} \sin\left(\frac{n\pi x}{L}\right) \tag{70}$$

APPENDIX-B

Determination of Tether Stiffness

For small displacements of tunnel in horizontal and vertical direction, analytical expression for tether stiffness has been formulated in this appendix. For the analysis purpose the length of the tethers considered is L , area of cross-section is A , modulus of Elasticity of Steel is E , angle of inclination of tethers is θ and the initial pretension in the tethers is T_0 . The displacement δx and δz of the structure in horizontal and vertical direction respectively is assumed to be very small.

Case-1 Vertical Tethers Stiffness for Sway Motion

In Figure 44 for the displacement of structure in horizontal direction, the change in tether tension can be written as

$$\Delta T_x = \frac{AE}{L}\left(\sqrt{\delta_x{}^2 + L^2} - L\right) \tag{71}$$

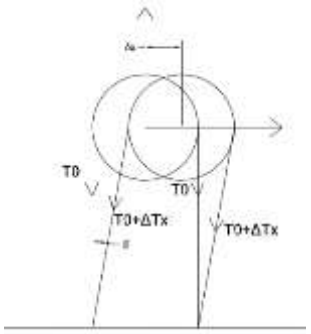

Figure 44 Sway motion of vertically tethered tunnel

On applying the force equilibrium condition in horizontal direction we obtain,

$$k_x \delta_x = 2\left(T_0 + \Delta T_x\right)\sin\left(\beta\right) \tag{72}$$

$$\sin(\beta) = \frac{\delta_x}{\sqrt{\delta_x^{\,2} + L^2}} \tag{73}$$

Substituting Eq.(71) and Eq.(73) in to Eq.(72) we get

$$k_x = \frac{2T_0}{\sqrt{\delta_x^{\,2} + L^2}} + \frac{2AE}{L}\left(1 - \frac{L}{\sqrt{\delta_x^{\,2} + L^2}}\right) \tag{74}$$

For very small δ_x Eq.(74) can be simplified as

$$k_x = \frac{2T_o}{L} \tag{75}$$

Case-2 Vertical Tethers Stiffness for Heave Motion

For the displacement of structure in vertical direction as shown in Figure 45, the change in tether tension can be expressed as

$$\Delta T_z = \frac{AE}{L}\delta_z \tag{76}$$

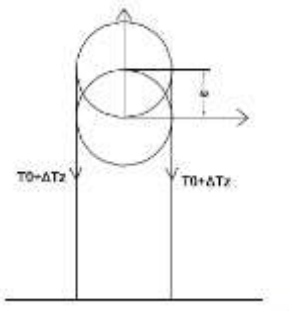

Figure 45 Heave motion of vertically tethered tunnel

Applying force equilibrium in vertical direction gives

$$k_z\delta_z = 2\left(T_0 + \Delta T_z\right) - 2T_0 \tag{77}$$

Substituting ΔT_z in Eq.(76) gives

$$k_z = \frac{2AE}{L} \tag{78}$$

Case-3 Inclined Tether Stiffness for Sway Motion

For inclined tethers for displacement in horizontal direction as shown in Figure 46, the change in tether tension can be written as

$$\Delta T_x = \frac{AE}{L}\Delta L \tag{79}$$

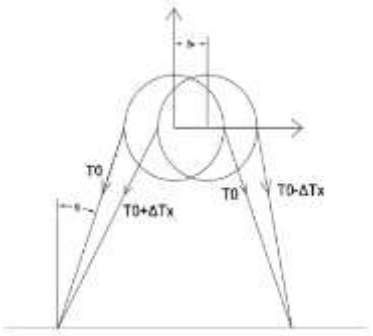

Figure 46 Sway motion of inclined tethered tunnel

Where ΔL is the change in the length of the tether and is related to horizontal displacement δ_x by

$$\Delta L = \delta_x \sin(\theta) \tag{80}$$

Applying force equilibrium in horizontal direction gives

$$k_x \delta_x = (T_0 + \Delta T_x)\sin\theta - (T_0 - \Delta T_x)\sin\theta \tag{81}$$

Substituting Eq.(79) and Eq.(80) in Eq.(81) we get

$$k_x = \frac{2AE}{L}\sin^2\theta \tag{82}$$

Case-4 Inclined Tether Stiffness for Heave Motion

For inclined tethers for displacement in horizontal direction as shown in Figure 47, the change in tether tension can be written as

$$\Delta T_z = \frac{AE}{L}\Delta L \tag{83}$$

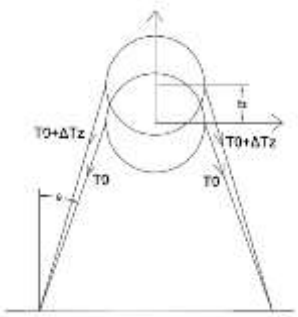

Figure 47 Heave motion for inclined tether tunnel

Where ΔL is the change in the length of the tether and is related to horizontal displacement δ_x by

$$\Delta L = \delta_z \cos(\theta) \tag{84}$$

Applying force equilibrium in horizontal direction gives

$$k_z \delta_z = 2(T_0 + \Delta T_z)\cos\theta - 2T_0 \cos\theta \tag{85}$$

Substituting Eq.(83) and Eq.(84) in Eq.(85) we get

$$k_z = \frac{2AE}{L}\cos^2\theta \tag{86}$$

APPENDIX-C

Solution of Governing Equation for Euler-Bernoulli Beam on Continuous Elastic Foundation

For a beam resting on continuous elastic foundation the governing partial differential equation of motion can be written as [29, 31]

$$EI\frac{\partial^4 v(x,t)}{\partial x^4}+m\frac{\partial^2 v(x,t)}{\partial t^2}+k_s v(x,t)=F(x,t) \tag{87}$$

For free vibration analysis the forcing term on right-hand side is equated to zero. Using the method of separation of variable the solution $v(x,t)$ of the governing equation can be written in the form,

$$v(x,t)=\Phi_n(x)V_n(t) \tag{88}$$

Substituting Eq.(88) in to Eq.(87) gives

$$EI\Phi_n''''(x)V_n(t)+k_s\Phi_n(x)V_n(t)=-m\Phi_n(x)\ddot{V}_n(t) \tag{89}$$

which can further be written as

$$\frac{EI\Phi_n''''(x)+k_s\Phi_n(x)}{m\Phi_n(x)}=-\frac{\ddot{V}_n(t)}{V_n(t)}=\omega_n^2 \tag{90}$$

where ω_n is a constant.

Eq.(90) can now be separated into two ordinary differential equations in $\Phi_n(x)$ and $V_n(t)$ and the equations are

$$EI\Phi_n''''(x)-\left(m\omega_n^2-k_s\right)\Phi_n(x)=0 \tag{91}$$

$$\ddot{V}_n(t) + \omega_n^2 V_n(t) = 0 \tag{92}$$

Generalized solutions of Eq.(91) and Eq.(92) are

$$V_n(t) = A\sin(\omega_n t - \beta_n) \tag{93}$$

$$\Phi_n(x) = C_1\cosh(\alpha_n x) + C_2\sinh(\alpha_n x) + C_3\cos(\alpha_n x) + C_4\sin(\alpha_n x) \tag{94}$$

where

$$\alpha_n^4 = \frac{m\omega_n^2 - k_s}{EI}$$

Using the boundary conditions of a simply supported beam, the constants of Eq.(94) are determined and further simplified to get

$$C_4\sin(\alpha_n L) = 0 \tag{95}$$

For Eq.(95) to have non-trivial solutions

$$\sin(\alpha_n L) = 0$$

$$\alpha_n = \frac{n\pi}{L} \tag{96}$$

Using solution of Eq.(94), the natural frequency of vibration of a beam resting on elastic foundation is determined and is given as

$$\omega_n = \sqrt{\left(\frac{n\pi}{L}\right)^4 \frac{EI}{m} + \frac{k_s}{m}} \tag{97}$$

Furthermore, the natural modes of vibration of beam are found to be similar to the case of freely spanning tunnel without any intermediate support and are

$$\Phi_n(x) = C_4 \sin\left(\frac{n\pi x}{L}\right) \tag{98}$$

Furthermore, using the property of orthogonality of modes and normalizing the modes

$$\Phi_n(x) = \sqrt{\frac{2}{mL}} \sin\left(\frac{n\pi x}{L}\right) \tag{99}$$

APPENDIX-D

Dynamic Stiffness Formulation for Beam on Discrete Elastic Supports

For Euler-Bernoulli beam the element dynamic stiffness matrix relating the nodal forces and displacement is given as [38, 39]

$$\begin{bmatrix} fy_1 \\ m_1 \\ fy_2 \\ m_2 \end{bmatrix} = \begin{bmatrix} d_1 & d_2 & d_4 & d_5 \\ d_2 & d_3 & -d_5 & d_6 \\ d_4 & -d_5 & d_1 & -d_2 \\ d_5 & d_6 & -d_2 & d_3 \end{bmatrix} \begin{bmatrix} \delta y_1 \\ \theta_1 \\ \delta y_2 \\ \theta_2 \end{bmatrix} \tag{100}$$

where f is the nodal force matrix, $K(\omega)$ is the frequency dependent dynamic stiffness matrix and δ is the nodal displacement matrix.

Using the element dynamic stiffness matrix $K(\omega)$, the global stiffness matrix of a three span tethered SFT with tethers treated as discrete elastic supports, is assembled

The multispan system is divided into three elements as shown in Figure 48 and Figure 49 and the dynamic stiffness matrix is formulated for each span.

For element 1,

$$\begin{bmatrix} fy_1 \\ m_1 \\ fy_2 \\ m_2 \end{bmatrix} = \begin{bmatrix} d_1 & d_2 & d_4 & d_5 \\ d_2 & d_3 & -d_5 & d_6 \\ d_4 & -d_5 & d_1 & -d_2 \\ d_5 & d_6 & -d_2 & d_3 \end{bmatrix} \begin{bmatrix} \delta y_1 \\ \theta_1 \\ \delta y_2 \\ \theta_2 \end{bmatrix} \tag{101}$$

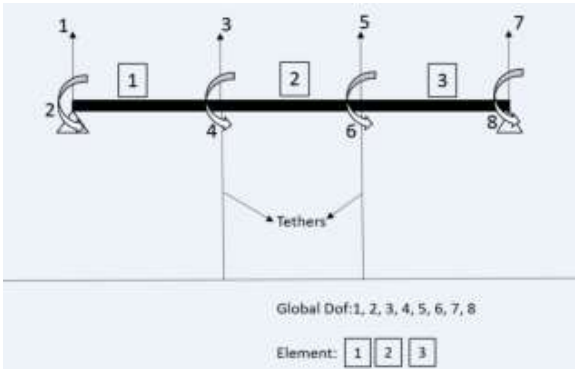

Figure 48 Global model of a three span floating tunnel

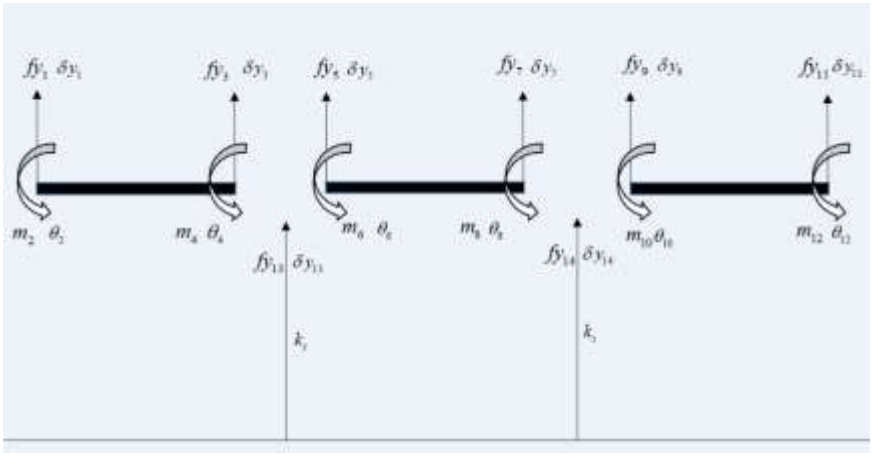

Figure 49 Local degrees of freedom for three span floating tunnel

For element 2,

$$\begin{bmatrix} fy_5 \\ m_6 \\ fy_7 \\ m_8 \end{bmatrix} = \begin{bmatrix} d_1 & d_2 & d_4 & d_5 \\ d_2 & d_3 & -d_5 & d_6 \\ d_4 & -d_5 & d_1 & -d_2 \\ d_5 & d_6 & -d_2 & d_3 \end{bmatrix} \begin{bmatrix} \delta y_5 \\ \theta_6 \\ \delta y_7 \\ \theta_8 \end{bmatrix} \tag{102}$$

For element 3,

$$\begin{bmatrix} fy_9 \\ m_{10} \\ fy_{11} \\ m_{12} \end{bmatrix} = \begin{bmatrix} d_1 & d_2 & d_4 & d_5 \\ d_2 & d_3 & -d_5 & d_6 \\ d_4 & -d_5 & d_1 & -d_2 \\ d_5 & d_6 & -d_2 & d_3 \end{bmatrix} \begin{bmatrix} \delta y_9 \\ \theta_{10} \\ \delta y_{11} \\ \theta_{12} \end{bmatrix} \tag{103}$$

For spring elements,

$$[fy_{13}] = [k_s][\delta y_{13}] \tag{104}$$

$$[fy_{14}] = [k_s][\delta y_{14}] \tag{105}$$

Local element stiffness matrix of element 1, 2, 3 and spring elements is further assembled to get the global stiffness matrix,

$$[K(\omega)]_{global} = \begin{bmatrix} d_3 & -d_5 & d_6 & 0 & 0 & 0 \\ -d_5 & 2d_1 + k_s & 0 & d_4 & d_5 & 0 \\ d_6 & 0 & 2d_3 & -d_5 & d_6 & 0 \\ 0 & d_4 & -d_5 & 2d_1 + k_s & 0 & d_5 \\ 0 & d_5 & d_6 & 0 & 2d_3 & d_6 \\ 0 & 0 & 0 & d_5 & d_6 & d_3 \end{bmatrix} \tag{106}$$

APPENDIX-E

Solution of Governing Equations for Coupled Bending-Torsion behavior of Beam

For the case of coupled bending-torsion vibration of tunnel cross-section, the governing partial differential equation of motion is given by [31]

$$\left(EI\right)_{eff}\frac{\partial^4 v}{\partial x^4}+\rho_{eff}A\frac{\partial^2\left(v+\mathrm{e}\phi\right)}{\partial t^2}=f\left(x,t\right) \tag{107}$$

$$-\left(GJ\right)_{eff}\frac{\partial^2\phi}{\partial x^2}+\rho_{eff}I_p\frac{\partial^2\phi}{\partial t^2}+\rho_{eff}Ae\frac{\partial^2\left(v+e\phi\right)}{\partial t^2}=f\left(x,t\right)e \tag{108}$$

For finding the mode shapes and natural frequency of vibration of structure, a free vibration analysis of structure is carried out using the method of separation of variable.

Under the assumption that the beam is undergoing harmonic oscillations the solution $v(x,t)$ and $\phi(x,t)$ of the governing differential equations is assumed of the form,

$$v\left(x,t\right)=V\left(x\right)\sin\left(\omega t\right) \tag{109}$$

$$\phi\left(x,t\right)=\Phi\left(x\right)\sin\left(\omega t\right) \tag{110}$$

Substituting $v(x,t)$ and $\phi(x,t)$ in Eq.(107) and Eq.(108) gives,

$$\left(EI\right)_{eff}\frac{\partial^4 V}{\partial x^4}=\rho_{eff}A\omega^2\left(V+e\Phi\right) \tag{111}$$

$$-\left(GJ\right)_{eff}\frac{\partial^2\Phi}{\partial x^2}=\rho_{eff}I_p\omega^2\Phi+\rho Ae\omega^2\left(V+e\Phi\right) \tag{112}$$

Under the assumption that the tunnel is simply supported at the shores, the boundary conditions imposed on displacement and torsional rotation are,

At $x=0$ $\qquad V\left(x\right)=0 \qquad \Phi\left(x\right)=0$

$$(EI)_{eff} V''(x) = 0 \qquad (GJ)_{eff} \Phi''(x) = 0$$

At $x = L$ $\qquad V(x) = 0 \qquad \Phi(x) = 0$

$$(EI)_{eff} V''(x) = 0 \qquad (GJ)_{eff} \Phi''(x) = 0$$

The following functions can be seen to satisfy the boundary conditions,

$$V_n(x) = A_n \sin\left(\frac{n\pi x}{L}\right) \tag{113}$$

$$\Phi_n(x) = B_n \sin\left(\frac{n\pi x}{L}\right) \tag{114}$$

Substituting Eq.(113) and Eq.(114) in Eq.(111) and Eq.(112) we obtain,

$$(EI)_{eff} A_n \left(\frac{n\pi}{L}\right)^4 = \rho_{eff} A \omega_n^2 (A_n + eB_n) \tag{115}$$

$$(GJ)_{eff} B_n \left(\frac{n\pi}{L}\right)^2 = \rho_{eff} I_p \omega_n^2 B_n + \rho_{eff} A \omega_n^2 e (A_n + eB_n) \tag{116}$$

Eq.(115) and Eq.(116) can be rearranged and written as,

$$\left(p^2 - \omega_n^2\right) \mathrm{A}_n - \left(e\omega_n^2\right) \mathrm{B}_n = 0 \tag{117}$$

$$\left(q^2 \omega_n^2\right) \mathrm{A}_n - \left(r^2 - \omega_n^2\right) B_n = 0 \tag{118}$$

where

$$p^2 = \frac{(EI)_{eff}}{\rho_{eff} A} \left(\frac{n\pi}{L}\right)^4$$

$$q^2 = \frac{Ae}{I_p + Ae^2}$$

$$r^2 = \frac{(GJ)_{eff}\left(\frac{n\pi}{L}\right)^2}{\rho_{eff}\left(I_p + Ae^2\right)}$$

For non-trivial solution of Eq.(117) and Eq.(118), the determinant of coefficient matrix must be equal to zero. This leads to

$$\begin{vmatrix} p^2 - \omega_n{}^2 & -\omega_n{}^2 e \\ q^2\omega_n{}^2 & -\left(r^2 - \omega_n{}^2\right) \end{vmatrix} = 0 \tag{119}$$

On expanding Eq.(119) we get

$$\omega_j{}^4\left(q^2 e - 1\right) + \omega_j{}^2\left(p^2 + r^2\right) - p^2 r^2 = 0 \tag{120}$$

and

$$\omega_j{}^2 = \frac{\left(p^2 + r^2\right) \mp \sqrt{\left(p^2 + r^2\right) + 4p^2 r^2\left(q^2 e - 1\right)}}{2\left(1 - q^2 e\right)} \tag{121}$$

APPENDIX-F

Regular Waves-First Order (Linear) Approximation

Consider monochromatic (single frequency) regular (constant amplitude) waves propagating in water of constant depth h in the positive x-direction. Assume there are no obstructions to the waves.

Under the assumption that wave amplitude is small and wave steepness is low, the solution of the boundary value problem yields the first order velocity potential ϕ expressed as

$$\phi^{(1)} = \frac{gH}{2\omega}\frac{\cosh\left(k\left(z+h\right)\right)}{\cosh\left(kh\right)}\sin\left(kx-\omega t\right) \tag{122}$$

where H is the wave height, ω is the wave frequency, k is the wave number and z is the depth from free surface.

The first order pressure is obtained from the first order Bernoulli equation for $z \le 0$

$$p^{(1)}\left(x,z,t\right) = -\rho\frac{\partial\phi^{(1)}}{\partial t} = \rho g\frac{H}{2}\frac{\cosh\left(k\left(z+h\right)\right)}{\cosh\left(kh\right)}\cos\left(kx-\omega t\right) \tag{123}$$

In deep water, $kh >> \pi$, $\cosh\left(kh\right) \to e^{kh}/2$ and, except near the vicinity of the bottom where $z = -h$,

$$\cosh\left(k\left(z+h\right)\right) \to \frac{e^{k(z+h)}}{2}$$

So the first order dynamic pressure varies as

$$p^{(1)} = \rho g\frac{H}{2}e^{kz}\cos\left(kx-\omega t\right) \tag{124}$$

In shallow water, $kh < \pi/10$, $\cosh(kh) \to 1$ and $\cosh(k(z+h)) \to 1$, giving first order pressure as

$$p^{(1)} = \rho g \frac{H}{2} \cos(kx - \omega t) = \rho g \eta \tag{125}$$

that is, the total dynamic pressure for shallow water is given by

$$p = \rho g (\eta - z) \tag{126}$$

The first-order velocities and accelerations for fluid particles are

$$v^{(1)}{}_{wz} = \frac{\partial \phi^{(1)}}{\partial z} = \frac{gH}{2\omega} k \frac{\sinh(k(z+h))}{\cosh(kh)} \sin(kx - \omega t) \tag{127}$$

$$v^{(1)}{}_{wx} = \frac{\partial \phi^{(1)}}{\partial x} = \frac{gH}{2\omega} k \frac{\cosh(k(z+h))}{\cosh(kh)} \cos(kx - \omega t) \tag{128}$$

$$a^{(1)}{}_{wz} = \frac{\partial v^{(1)}{}_{wz}}{\partial t} = -\frac{gH}{2} k \frac{\sinh(k(z+h))}{\cosh(kh)} \cos(kx - \omega t) \tag{129}$$

$$a^{(1)}{}_{wx} = \frac{\partial v^{(1)}{}_{wx}}{\partial t} = \frac{gH}{2} k \frac{\cosh(k(z+h))}{\cosh(kh)} \sin(kx - \omega t) \tag{130}$$